© 2016. Published by The Company of Biologists Ltd | Development (2016) 143, 1571-1584 doi:10.1242/dev.125351

RESEARCH ARTICLE

Loss of Bmi1 causes anomalies in retinal development and degeneration of cone photoreceptors

Andrea Barabino[1,*], Vicky Plamondon[1,*], Mohamed Abdouh[1], Wassim Chatoo[1], Anthony Flamier[1], Roy Hanna[1], Shufeng Zhou[1], Noboru Motoyama[2], Marc Hébert[3], Joëlle Lavoie[3] and Gilbert Bernier[1,4,5,‡]

ABSTRACT

Retinal development occurs through the sequential but overlapping generation of six types of neuronal cells and one glial cell type. Of these, rod and cone photoreceptors represent the functional unit of light detection and phototransduction and are frequently affected in retinal degenerative diseases. During mouse development, the Polycomb group protein Bmi1 is expressed in immature retinal progenitors and differentiated retinal neurons, including cones. We show here that Bmi1 is required to prevent post natal degeneration of cone photoreceptors and bipolar neurons and that inactivation of Chk2 or p53 could improve but not overcome cone degeneration in *Bmi1*$^{-/-}$ mice. The retinal phenotype of *Bmi1*$^{-/-}$ mice was also characterized by loss of heterochromatin, activation of tandem repeats, oxidative stress and Rip3-associated necroptosis. In the human retina, BMI1 was preferentially expressed in cones at heterochromatic foci. BMI1 inactivation in human embryonic stem cells was compatible with retinal induction but impaired cone terminal differentiation. Despite this developmental arrest, BMI1-deficient cones recapitulated several anomalies observed in *Bmi1*$^{-/-}$ photoreceptors, such as loss of heterochromatin, activation of tandem repeats and induction of *p53*, revealing partly conserved biological functions between mouse and man.

KEY WORDS: Polycomb, Bmi1, Retina, Retinal development, Bipolar neuron, Cone, Photoreceptor, Degeneration, Mouse, Human, Embryonic stem cell

INTRODUCTION

The distinct competence of retinal progenitor cells (RPCs) to generate in a sequential order the diverse class of neurons and a single glial cell type during retinal development is thought to be modulated by an intrinsic transcription factor molecular program and by extrinsic cues (Belecky-Adams et al., 1996; Cepko et al., 1996; Reh and Kljavin, 1989; Watanabe and Raff, 1990). Loss- and gain-of-function studies in model organisms have revealed that the transcription factors Pax6, Rax (also called Rx), Lhx2, Otx2, Sox2, Six6 and Six3 are involved in early eye patterning and retinal developmental processes (Bernier et al., 2000; Carl et al., 2002; Chow et al., 1999; Lagutin et al., 2003; Loosli et al., 1999; Marquardt et al., 2001; Mathers et al., 1997; Porter et al., 1997; Taranova et al., 2006). Later on, specific sets of transcription factors define retinal cell type identity, including photoreceptors (Swaroop et al., 2010). Photoreceptor progenitor and precursor cells express Otx2 and Crx, and conditional deletion of *Otx2* in the developing mouse retina impairs photoreceptors fate (Nishida et al., 2003). In turn, Crx is required for terminal differentiation and maintenance of photoreceptors and is mutated in human retinal degenerative diseases (Chen et al., 1997; Freund et al., 1997, 1998; Furukawa et al., 1997, 1999; Swaroop et al., 1999). Photoreceptors exist as two cell types – rods and cones. Rods are involved in low-intensity night vision and cones are involved in high-intensity color vision. During development, photoreceptors follow an S-cone (cones containing S-opsin) default pathway, which is determined by cone-rod homeobox (Crx) and thryroid receptor β2 (Thrβ2, encoded by *Thrb*); Crx induces expression of *Opn1sw* (encoding S-opsin) by default, whereas Thrβ2 suppresses it and induces expression of *Opn1mw* (encoding M-opsin) (Ng et al., 2001; Yanagi et al., 2002). In turn, expression of neural retina leucine zipper (*Nrl*), RAR-related orphan receptor β (*Rorb*) and *Notch1* inhibit cone formation, whereas both Nrl and RORβ promote rod genesis at the expense of cones (Jadhav et al., 2006; Jia et al., 2009; Mears et al., 2001; Yaron et al., 2006).

Although the transcription factor dynamics controlling retinal development has been well described, the role of chromatin remodeling factors in retinal biology has been poorly explored (Hennig et al., 2013). Polycomb group proteins form large multimeric complexes that silence specific target genes by modifying chromatin organization (Valk-Lingbeek et al., 2004). The Polycomb group protein Bmi1 is a component of the polycomb repressive complex 1 (PRC1), which promotes chromatin compaction and gene repression through its mono-ubiquitin ligase activity on histone H2A at lysine 119 (Buchwald et al., 2006; Cao et al., 2005; Li et al., 2006). *Bmi1*$^{-/-}$ mice show axial skeleton defects, reduced post natal growth and lifespan, and progressive cerebellar degeneration (Jacobs et al., 1999; van der Lugt et al., 1994). Most Bmi1 functions in normal development and stem cell maintenance have been attributed to transcriptional repression of the *Cdkn2a* (also called the *INK4a/ARF*) locus, encoding p16^{INK4a} and p19^{ARF} (Sherr, 2001; Sharpless et al., 2004; Valk-Lingbeek et al., 2004). p16^{INK4a} is a cyclin-dependent kinase inhibitor that blocks the activity of Cdk4/6 by preventing its association with cyclin D, which results in Rb hypophosphorylation and cell cycle arrest or senescence. p19^{ARF} binds and inhibits the activity of the E3-ubiquitin ligase mouse double minute 2 (Mdm2), which prevents targeting of p53 for proteasomal degradation (Sherr, 2001; Sharpless et al., 2004). More recently, activation of the DNA damage response protein checkpoint kinase 2 (Chk2) was found to contribute to several pathologies found in *Bmi1*$^{-/-}$ mice (Liu et al., 2009). *Bmi1*$^{-/-}$ mice also develop a progeroid phenotype in the

[1]Stem Cell and Developmental Biology Laboratory, Hôpital Maisonneuve-Rosemont, 5415 Boul. l'Assomption, Montréal, Canada H1T 2M4. [2]Department of Cognitive Brain Science, National Institute for Longevity Sciences, National Center for Geriatrics and Gerontology, 36-3 Gengo, Morioka, Obu, Aichi 474-8522, Japan. [3]Department of Ophthalmology, Otorhinolaryngology and Cervico-Facial Surgery, Faculty of Medicine, Université Laval, Laval, Canada G1V 0A6. [4]Department of Neurosciences, Université de Montréal, Montréal, Canada H3T 1J4. [5]Department of Ophthalmology, Université de Montréal, Montréal, Canada H3T 1J4.
*These authors contributed equally to this work

‡Author for correspondence (gbernier.hmr@ssss.gouv.qc.ca)

Received 13 April 2015; Accepted 1 March 2016

Development (2016) 143, 1571-1584 doi:10.1242/dev.125351

CNS characterized by lens cataracts, cortical neurons apoptosis, p53 activation and accumulation of oxidative damage (Chatoo et al., 2009). In the developing retina, it was found that Bmi1 is not required for the proliferation of the main RPC population, but for proliferation and post natal maintenance of most immature RPCs located at the retinal ciliary margin. *Bmi1* overexpression in RPCs with short-term proliferating activity induces chromatin remodeling and conversion into long-term RPCs with stem cell characteristics (Chatoo et al., 2010). *Bmi1* thus distinguishes most immature progenitor/stem cells from the main RPC population during retinal development (Chatoo et al., 2010). Notably, *Bmi1* is also expressed in differentiated retinal neurons, including photoreceptors, raising the possibility that it might be important for their post natal development or maintenance (Chatoo et al., 2009, 2010).

We report here that whereas retinal cell type genesis occurs relatively normally in *Bmi1*$^{-/-}$ mice, cone bipolar neurons and cone photoreceptors rapidly degenerate during post natal eye development through necroptosis. In the human retina, *BMI1* was preferentially expressed in cones and *BMI1* inactivation in human embryonic stem cells impaired *CRX* expression and cone terminal differentiation. The cellular phenotype was also associated with chromatin compaction anomalies, activation of tandem repeats and induction of *p53*, as found in *Bmi1*$^{-/-}$ mice. These findings revealed new and partly conserved biological functions for Bmi1 during cone photoreceptor development between mouse and man.

RESULTS

To investigate a possible function of Bmi1 in retinal neurons differentiation, we performed immunohistochemistry (IHC) and immunofluorescence (IF) analyses on retinas from wild-type (WT) and *Bmi1*$^{-/-}$ littermates at post natal day 30 (P30). This revealed that retinal organization and cell type genesis were possibly perturbed in *Bmi1*$^{-/-}$ mice (Figs 1,2 and Figs S1,S2). The distribution of syntaxin, which labels amacrine neurons, was abnormal, resulting in its focal accumulation in the inner nuclear layer (Fig. 1A, Fig. S2). The distribution of S-opsin, which labels the outer segment of cones, was also perturbed (Fig. 1A, Fig. S1). By contrast, the overall intensity and distribution of rhodopsin, which labels the rod outer segment, was apparently normal. The total number of nuclei in the outer nuclear layer, which is a measure of the total number of photoreceptors (mostly rods), was also comparable between the two genotypes (Fig. 1A,B, Fig. S2). We quantified the number of all major retinal cell types using specific antibodies (Haverkamp and Wässle, 2000; Marquardt, 2003; Marquardt et al., 2001). We found that the number of ganglion, amacrine and horizontal cells was comparable between both genotypes (Fig. 1G,H, Fig. S2). However, the number of S-cones as well as rod bipolar (PKCα^{+}/Chx10^{+}) and cone bipolar (Chx10^{+}/PKCα^{-}) neurons was highly reduced in *Bmi1* mutants (Fig. 1B, Fig. 2A-C). Amongst the two subcategories of cone bipolar neurons, T2 ON and T8 OFF neurons (labeled by recoverin) were also nearly absent (Fig. 2G, Fig. S2).

To test whether the observed reduction in cone numbers in *Bmi1*$^{-/-}$ mice was the result of a developmental defect or secondary to degeneration, we compared P12 and P30 mice. On retinal flat mounts, we found that S-opsin^{+} and PNA^{+} cone cells were equally abundant in the ventro-nasal region of WT and *Bmi1*$^{-/-}$ mice at P12, but not at P30, thus suggesting cone degeneration (Fig. 1C-F, Fig. S1). The apparent over-representation of S-opsin in the ventro-nasal region, in contrast to the dorso-temporal region, is due to the dual nature of mouse cone photoreceptors, which frequently express both S-opsin and M-ospin (Fig. S4A) (Ortín-Martínez et al., 2014). These analyses also highlighted a significant reduction in cone numbers in *Bmi1*$^{+/-}$ mice, revealing a gene-dosage effect (Fig. 1C,D). We performed labeling with an antibody against activated caspase-3 to test for apoptosis. Positive cells were, however, not observed in either WT or *Bmi1*$^{-/-}$ retinas at P30, suggesting that apoptosis is not the main mechanism of retinal cell death in *Bmi1*$^{-/-}$ mice (data not shown). This is consistent with our previous findings, where differences in the number of caspase-3^{+} cells were not observed between WT and *Bmi1*$^{-/-}$ retinas at P6 (Chatoo et al., 2010). To test for an altered retinal differentiation program, we performed quantitative RT-PCR (qPCR) on retinal extracts. Although expression of the Bmi1-repressed locus *Cdkn2a* (encoding the *p16*^{INK4a} and *p19*^{ARF} transcripts) was increased in *Bmi1*$^{-/-}$ retinas (Fig. 2I) (Molofsky et al., 2005), no difference in the expression level of several retinal determination genes was observed between the two genotypes.

We also investigated *Bmi1* expression in the WT mouse retina at P30. Although *Bmi1* was expressed in nearly all retinal cell types, it was most abundant in Chx10^{+} bipolar neurons (Fig. S5). In the outer nuclear layer, it was predominant in cones, not in rods, as further shown using the cone-only retina of *Nrl* null mice (Fig. S3A) (Mears et al., 2001). To test whether the cone degeneration phenotype was cell autonomous, we performed dissociated retinal cultures from WT and *Bmi1*$^{-/-}$ mice at P1. Although the percentage of S-cones was comparable after 4 days *in vitro* (DIV) between both genotypes, as revealed using Bmi1 and S-opsin immunolabeling (Fig. S3B,C), it was highly reduced in *Bmi1*$^{-/-}$ cultures after 8 DIV and 12 DIV, suggesting cell-autonomous degeneration of cones (Fig. S3C). Taken together, these observations revealed predominant expression of Bmi1 in retinal neurons that degenerate in *Bmi1*$^{-/-}$ mice.

Cone function is severely perturbed in *Bmi1*$^{-/-}$ mice

To test the visual function, we performed electroretinogram (ERG) recordings of mouse retinal activity at P30. Examination of the ERG traces for the cone system revealed that cone activity was severely affected in *Bmi1*$^{-/-}$ mice when compared with WT (Fig. 3A-C). Notably, we observed a dose-dependent effect as cone activity was also perturbed in *Bmi1*$^{+/-}$ mice. When tracing the luminance response functions (LRFs), significant genotype-dependent differences were observed between WT, *Bmi1*$^{+/-}$ and *Bmi1*$^{-/-}$ mice for all four ERG parameters in the photopic condition, namely the a-wave amplitude ($F_{2,7}$=6.195, P=0.028; Fig. 3B, Table S1), the b-wave amplitude ($F_{2,7}$=18.970, P=0.001; Fig. 3C, Table S1), the a-wave implicit time ($F_{2,7}$=5.127, P=0.043; Table S1) and the b-wave implicit time ($F_{2,7}$=20.852, P=0.001; Table S1). These results suggest that cone photoreceptor activity, as measured with the a-wave, and the cone bipolar cell activity, as measured with the b-wave, were severely altered in *Bmi1*$^{-/-}$ mice. Also, the rod system was affected in *Bmi1*$^{-/-}$ mice, as observed by the lower b-wave amplitude when compared with WT mice, but the difference was not significant for *Bmi1*$^{+/-}$ mice (Fig. 3D-F, Table S1). When analyzing the LRFs, only the b-wave amplitude was found to be significantly different between WT and *Bmi1*$^{-/-}$ mice ($F_{2,7}$=10.440, P=0.008; Fig. 3F, Table S1), suggesting that rod bipolar cell activity was affected in *Bmi1*$^{-/-}$ mice, but at a lower level than in photopic conditions (Fig. 3C).

Loss of heterochromatin and necroptosis in *Bmi1*$^{-/-}$ cones

We next analyzed the retina of *Bmi1*$^{-/-}$ mice by transmission electron microscopy (TEM) to search for ultrastructural anomalies at P30. In WT mice, the electron-dense heterochromatin of rods was pre-eminent, located in the center of the nucleus and

Development (2016) 143, 1571-1584 doi:10.1242/dev.125351

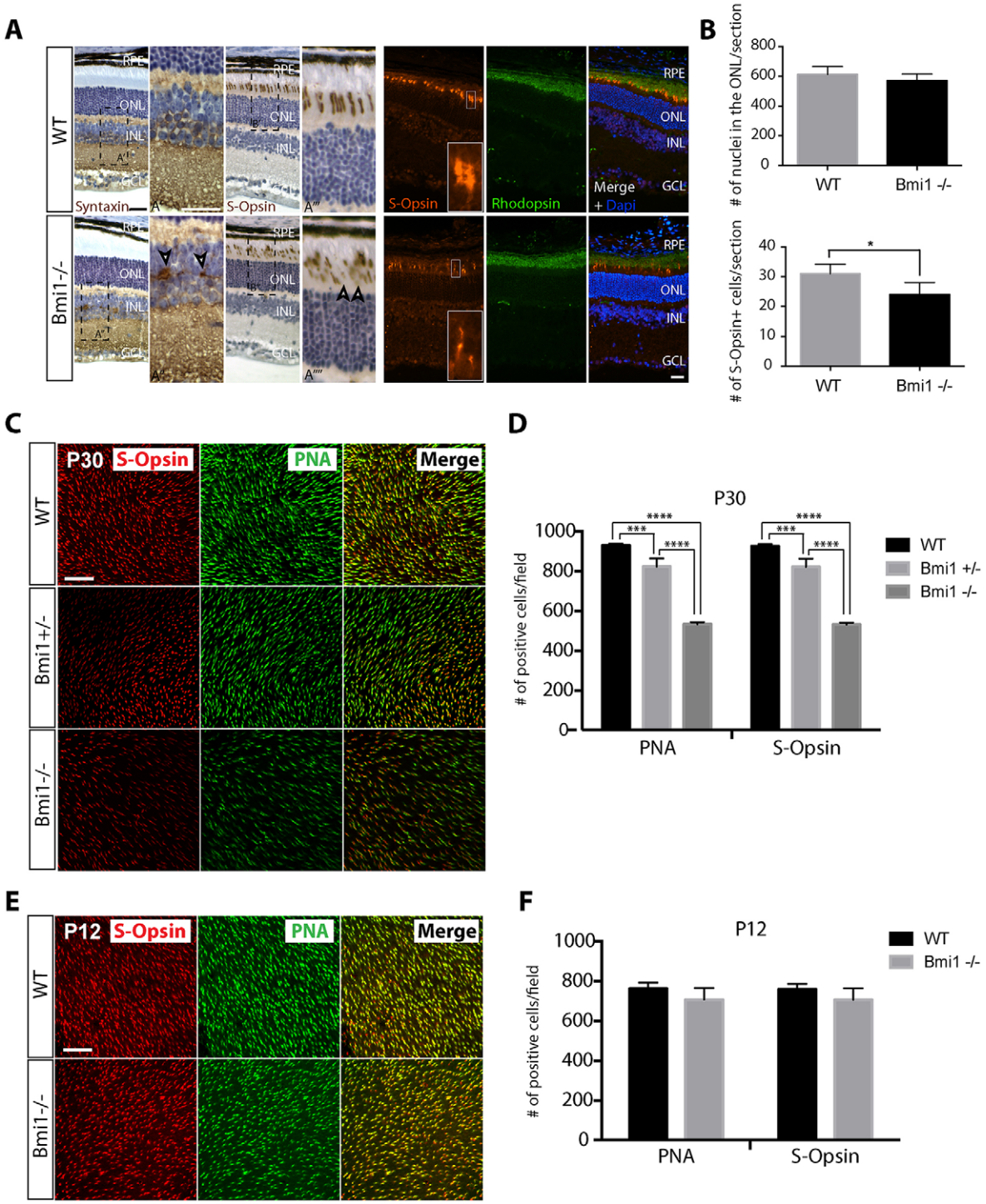

Fig. 1. S-cones degenerate during post natal eye development in *Bmi1*$^{-/-}$ mice. (A) Analyses of WT and *Bmi1*$^{-/-}$ retinas at P30. Abnormal distribution of syntaxin (arrowheads in A″) and cone photoreceptor outer segments breaks in *Bmi1*$^{-/-}$ mice (arrowheads in A‴) as visualized by IHC. Cone photoreceptor outer segments break but rod photoreceptors appear normal in *Bmi1*$^{-/-}$ mice, as visualized by IF. (B) Quantification of total number of photoreceptors (top) and S-cones (bottom). (C,E) Representative microscopy images from retinal flat-mount of WT, *Bmi1*$^{+/-}$ and *Bmi1*$^{-/-}$ mice at P30 (C) and WT and *Bmi1*$^{-/-}$ at P12 (E). Images were taken in the ventro-nasal part of the retina. (D,F) Quantification of S-cone photoreceptors (S-opsin^{+}) and total cone photoreceptors (PNA^{+}) at P30 (D) and P12 (F). RPE, retinal pigment epithelium; ONL, outer nuclear layer; INL, inner nuclear layer; GCL, ganglion cell layer. Scale bars: 40 µm. All values are means±s.e.m. *P≤0.05; ***P≤0.001; ****P≤0.0001; Student's *t*-test (B,F), two-way ANOVA (D).

generally organized as a single large chromocenter (Fig. 4A, gray arrows) (Solovei et al., 2009). By contrast, cone nuclei had 1-3 chromocenters that occupied a much-reduced nuclear surface (Fig. 4A, white arrows). Cone cell bodies were also located close to the junction with the inner segment, in contrast to rod cell bodies, which were evenly distributed in the outer nuclear layer (Fig. 4A, Fig. S3A). In *Bmi1*$^{-/-}$ mice, the nucleus of rods appeared normal but the chromocenter was slightly reduced in size

Development (2016) 143, 1571-1584 doi:10.1242/dev.125351

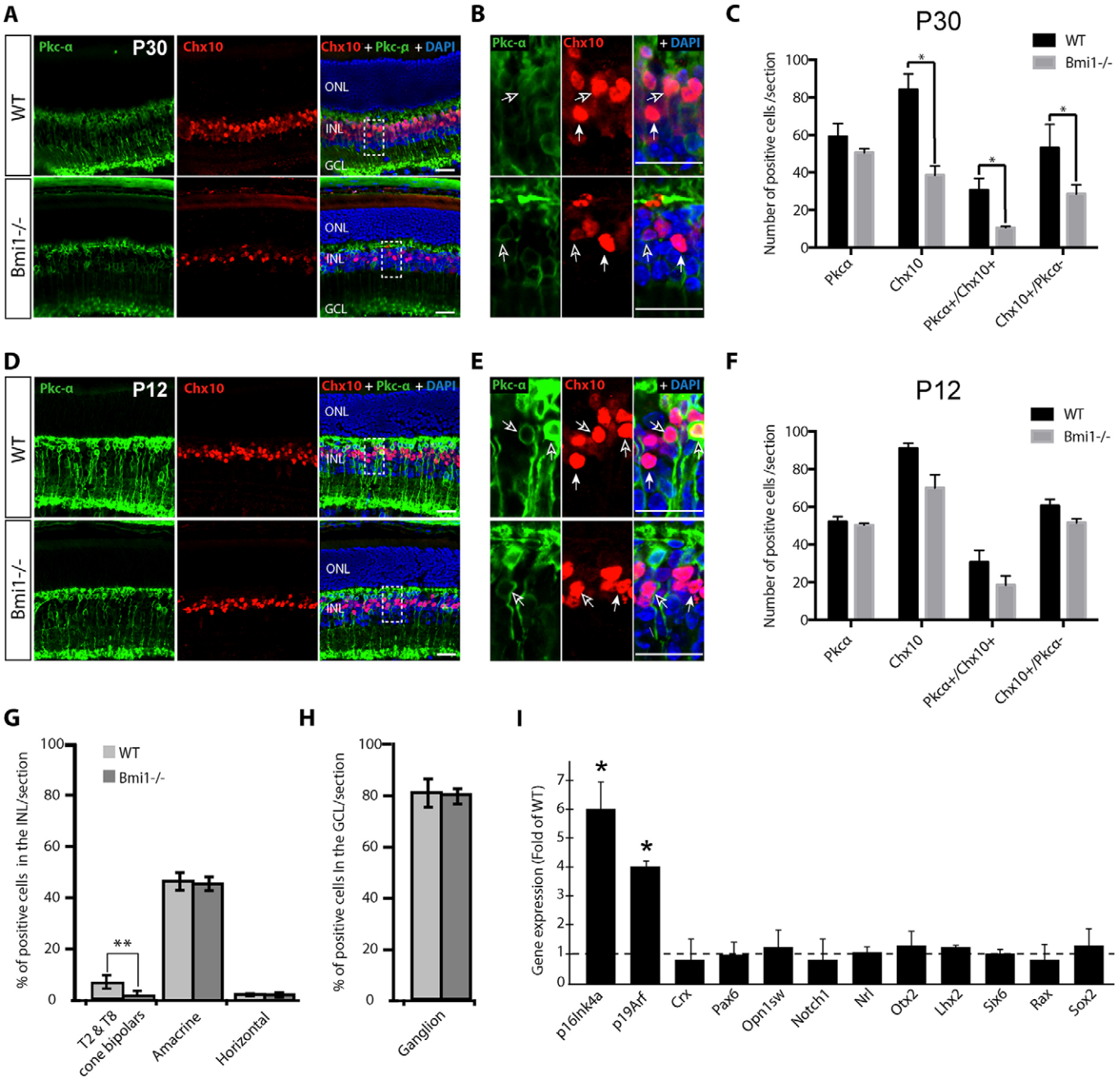

Fig. 2. Bipolar neurons degenerate during post natal eye development in *Bmi1*$^{-/-}$ mice. (A,D) Representative images of WT and *Bmi1*$^{-/-}$ retinas at P30 (A) and P12 (D) labeled with antibodies against PKCα and Chx10. (B,E) Cropped images indicated by the respective dashed rectangles indicated in A and D. White filled arrows: cone bipolar cells (Chx10^{+}/PKCα^{-}). White-edged arrows: rod bipolar cells (Chx10^{+}/PKCα^{+}). Note the decrease in Chx10^{+} cells in *Bmi1*$^{-/-}$ retinas at P30. (C,F) Quantification of data acquired in A and D. (G) Quantification of T2-OFF and T8-ON cone bipolar cells (Recoverin^{+}), amacrine cells (Pax6^{+}) and horizontal cells (Calbindin^{+}) in the INL. (H) Quantification of ganglion cells (Pax6^{+}) in the GCL. (I) Gene expression analysis of WT and *Bmi1*$^{-/-}$ retinas at P30, where *p16*^{INK4a} and *p19*^{ARF} were used as positive controls. RPE, retinal pigment epithelium; ONL, outer nuclear layer; INL, inner nuclear layer; GCL, ganglion cell layer. Scale bars: 40 µm. All values are means±s.e.m. *P≤0.05; **P≤0.01; Student's *t*-test.

and showed less condensation (Fig. 4B). The cell body, inner segment and outer segment of rods were apparently normal. By contrast, the cell bodies and nuclei of cones were swollen and highly degenerative (Fig. 4A, white arrows). Accumulation of swollen mitochondria and fibrous material in the cell body of cones was also observed, suggesting necrotic cell death (also known as necroptosis) (Fig. 4A, white and black arrows in the high-magnification image) (Linkermann and Green, 2014).

To further investigate the observed chromatin phenotype, we analyzed mice at P15, when chromatin condensation of immature rods is not yet completed. Marked differences in rod heterochromatin condensation could be observed between WT and *Bmi1*$^{-/-}$ mice by transmission electron microscopy (TEM) (Fig. 4B). Using retinal sections at P25 and antibodies against 'open' chromatin (H3K9ac), facultative heterochromatin (H3K27me3) and constitutive heterochromatin (H3K9me3), we found that the chromatin in the outer nuclear layer of *Bmi1*$^{-/-}$ mouse retinas was less condensed

Development (2016) 143, 1571-1584 doi:10.1242/dev.125351

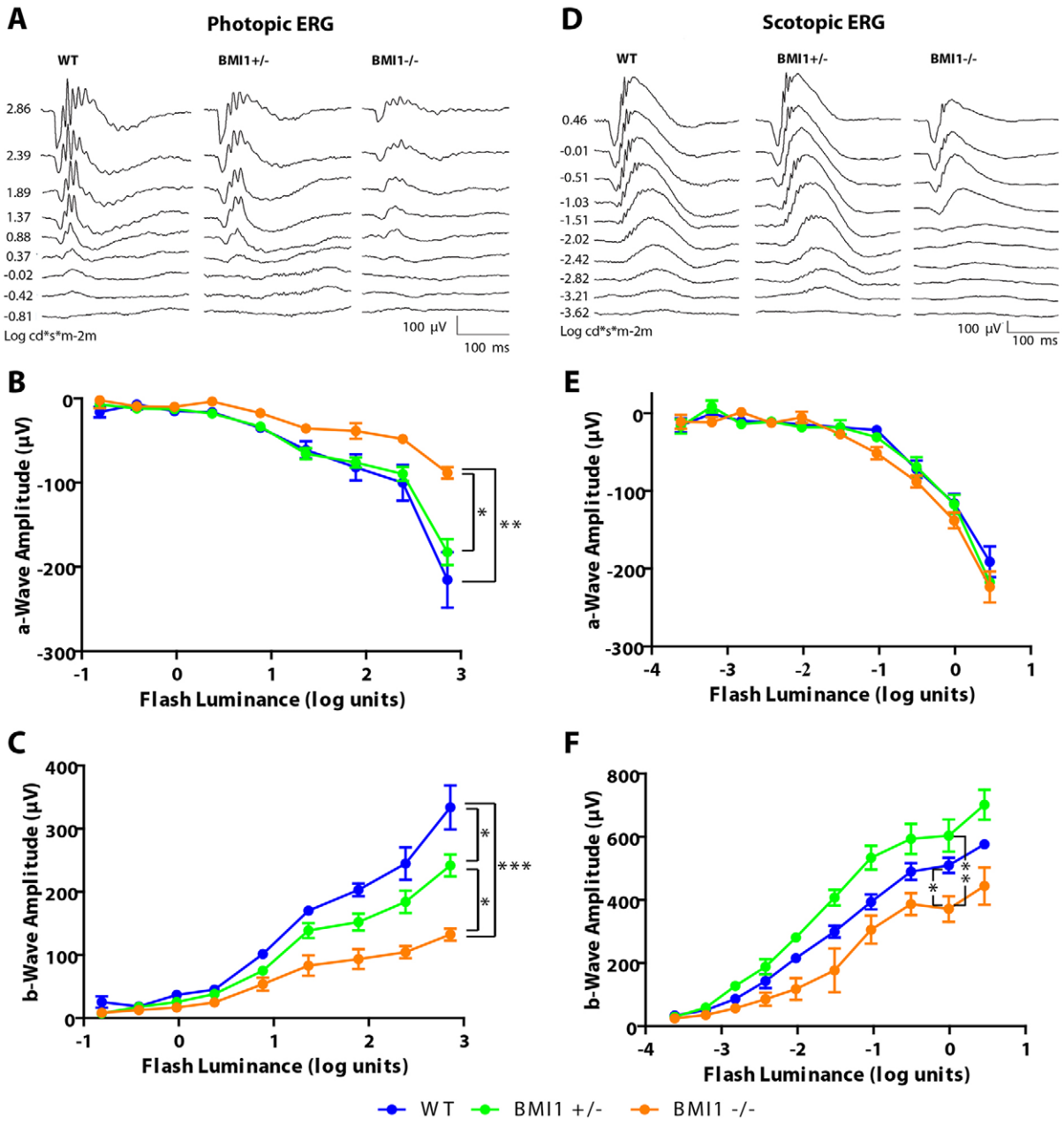

Fig. 3. Cone and rod function is severely perturbed in *Bmi1*$^{-/-}$ mice. ERG recorded in photopic (A-C) and scotopic (D-F) conditions. (A,D) ERG waveforms for WT, *Bmi1*$^{+/-}$ and *Bmi1*$^{-/-}$ mice. Luminance response function curve of a-wave (B,E) and b-wave (C,F) representing the dynamic electrical response from the cone (B,C) and rod (E,F) systems. Note the significant decrease in the retinal responses of *Bmi1*$^{+/-}$ mice and *Bmi1*$^{-/-}$ mice in photopic conditions for both the a-wave and b-wave amplitude at the V_{max} compared with WT mice and the decrease of the b-wave amplitude at the V_{max} in scotopic conditions in *Bmi1*$^{-/-}$ mice compared with WT and *Bmi1*$^{+/-}$ mice. All values are means±s.e.m. *P≤0.05; **P≤0.01; ***P≤0.001; one-way ANOVA.

when compared with that of WT mice (Fig. 4C) (Fodor et al., 2010). The intergenic and pericentromeric constitutive heterochromatin contains numerous repetitive DNA sequences of retroviral origin that can be transcribed but are generally silenced by heterochromatin formation (Fodor et al., 2010; Karimi et al., 2011). We thus compared the expression level of repetitive DNA sequences (Iap1, Line, Sine, major satellite repeats and minor satellite repeats) between retinas from WT and *Bmi1*$^{-/-}$ mice by qPCR using RNA extracts first treated with DNaseI, because these transcripts are intron-less. We found increased expression of all tested repetitive sequences in *Bmi1*$^{-/-}$ retinas, consistent with the reduced heterochromatin compaction phenotype (Fig. 4D).

To investigate the mechanism of cell death, we measured the expression of genes known to mediate necroptosis (Murakami et al., 2012; Vandenabeele et al., 2010; Viringipurampeer et al., 2014). We found that the mRNA level of receptor-interacting protein kinase 3 (*Ripk3*) was significantly increased in *Bmi1*$^{-/-}$ retinas when compared with WT (Fig. 5A). Rip3 protein accumulation in *Bmi1*$^{-/-}$ and *Bmi1*$^{+/-}$ retinas was confirmed by western blot analysis (Fig. 5B). In these preparations, we noticed that Rip3 accumulation could be readily observed upon Ponceau Red staining of the nitrocellulose membrane. Furthermore, protein accumulation was present at ∼20 kDa in *Bmi1*$^{-/-}$ retinal extracts, suggesting 'programmed' proteolytic cleavage (Fig. 5B). To

Development (2016) 143, 1571-1584 doi:10.1242/dev.125351

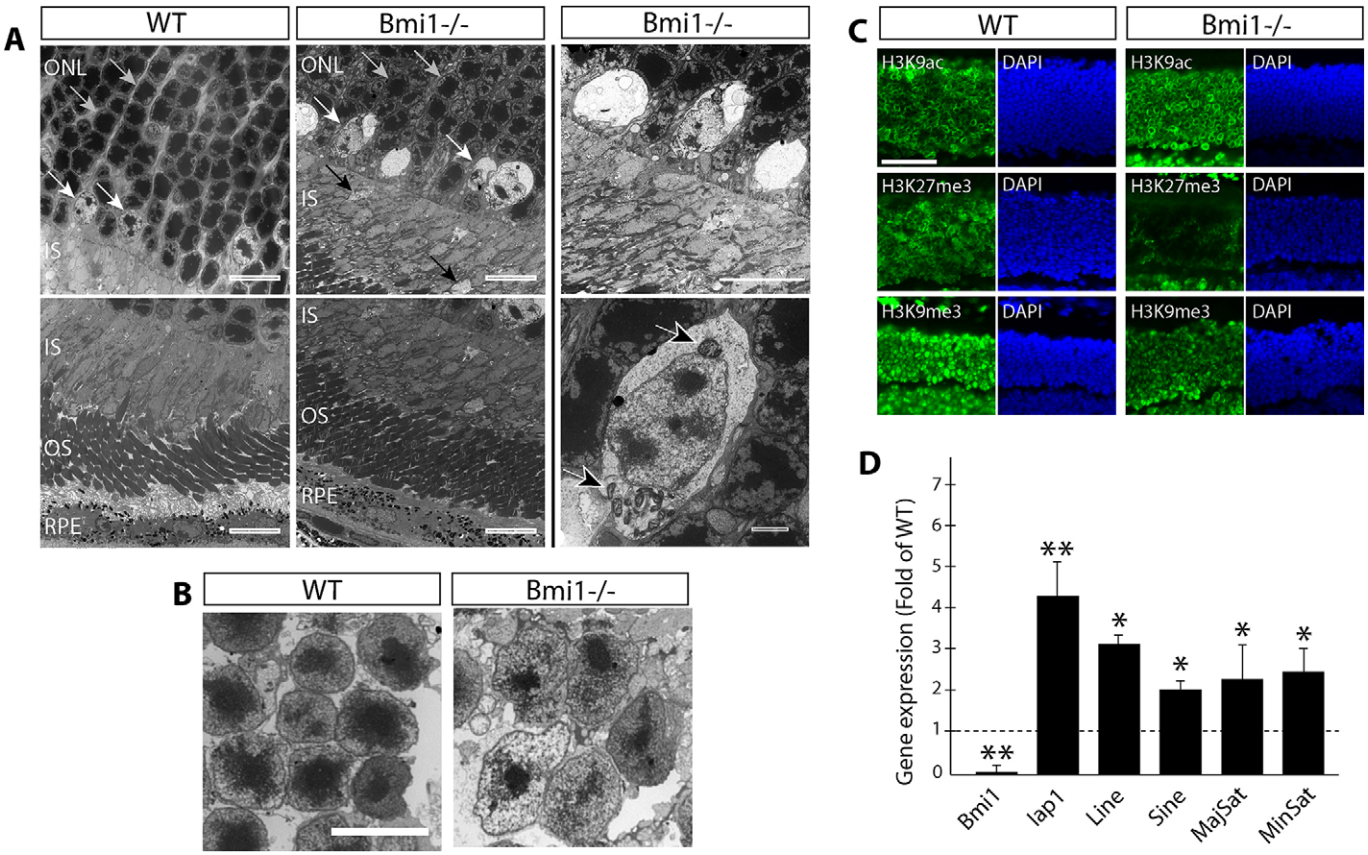

Fig. 4. Cone necrosis, loss of heterochromatin and activation of tandem repeats in *Bmi1*$^{-/-}$ mouse retinas. (A) TEM on WT and *Bmi1*$^{-/-}$ retinas at P30. White arrows, cone photoreceptors; gray arrows, rod photoreceptors characterized by electron-dense heterochromatin organized as a single chromocenter; black arrows, degenerative cone cell bodies; white-edged black arrows, swollen mitochondria in cones. (B) TEM analysis of WT and *Bmi1*$^{-/-}$ rod photoreceptors at P15. (C) Analysis of histone modifications in WT and *Bmi1*$^{-/-}$ retinas by IF on sections at P25. (D) Quantitative PCR analysis of expression of repetitive DNA sequences in WT and *Bmi1*$^{-/-}$ retinas at P30. *Bmi1* is used as a negative control and values are expressed as fold of WT value. RPE, retinal pigment epithelium; ONL, outer nuclear layer; OS, outer segment; IS, inner segment. Scale bars: 10 µm (A, left, center and top-right images); 2 µm (A, bottom-right image); 5 µm in B; 25 µm in C. All values are means±s.e.m. *P≤0.05; **P≤0.01; Student's *t*-test.

identify which retinal cell types were most affected, we performed immunofluorescence (IF) analyses on sections. In both P12 and P30 *Bmi1*$^{-/-}$ retinas, we observed Rip3 immunolabeling in cones, but not in rods, and in neurons located in the inner nuclear layer, thus possibly corresponding to bipolar neurons (Fig. 5C-G). Rip3 immunolabeling was observed in the cell body and outer segment of cones at P12 (Fig. 5E,F), but was predominant in the outer segment of cones at P30 (Fig. 5C,D). Morphological anomalies of the cone outer segment were also clearly visible in *Bmi1*$^{-/-}$ retinas at P30 (Fig. 5D). Taken together, these results reveal that necroptosis is the main mechanism of cone photoreceptors cell death in *Bmi1*$^{-/-}$ mice.

Chk2 or *p53* genetic deficiency can partially improve the *Bmi1*$^{-/-}$ retinal phenotype

To investigate additional molecular mechanisms leading to cone degeneration, we generated double null mutants for the *Bmi1* and *p16*^{INK4a}/*p19*^{ARF}, *p19*^{ARF} or *Chk2* alleles. As previously reported, the *p16*^{INK4a}/*p19*^{ARF} or *p19*^{ARF} mutant alleles did not rescue size or lifespan defects in *Bmi1* null mice (Molofsky et al., 2005). By contrast, insertion of the *Chk2* mutant allele improved size and lifespan in *Bmi1* null mice, although *Bmi1*$^{-/-}$/*Chk2*$^{-/-}$ mice remained smaller than normal (Fig. S6). Interestingly, the number of cones in *Bmi1* null retinas at P30 was significantly improved by the *Chk2* mutant allele, but not by the *p16*^{INK4a}/*p19*^{ARF}or *p19*^{ARF} mutant alleles (Fig. 6A,B). However, morphology of the cone outer segment remained highly abnormal in *Bmi1*$^{-/-}$/*Chk2*$^{-/-}$ mice (Fig. 6A). Hence, analysis of *Bmi1*$^{-/-}$/*Chk2*$^{-/-}$ mice at P150 revealed severe depletion of S-cones, suggesting that deletion of *Chk2* only provided a transitory rescue (Fig. 6C,D).

In cortical neurons of *Bmi1* null mice, stabilization of p53 leads to accumulation of reactive oxygen species (ROS) through repression of the *Nqo1*, *Gsta1* and *Sesn2* antioxidant genes (Chatoo et al., 2011, 2009). p53 also promotes neuronal cell death through activation of *Apaf1*, *Fas* and *Lpo* (Fortin et al., 2001) and Bmi1 was proposed to block ROS accumulation in blood cells and thymus through direct transcriptional repression of the pro-oxidant genes *Cyp24a1* and *Duox2* (Liu et al., 2009). By qPCR analysis on retinal extracts, we found that the expression of antioxidant genes in *Bmi1*$^{-/-}$ mice was unchanged or increased (*Nqo1*), whereas that of *Cyp24a1* and *Duox2* was increased (Fig. 7A). Notably, the expression of *Apaf1* and *Fas* was increased in *Bmi1*$^{-/-}$ retinas, consistent with the observed accumulation of p53 by western blot (Fig. 7B). Among 200 offspring, we obtained expected numbers of WT, *Bmi1*$^{+/+}$/*p53*$^{+/-}$, *Bmi1*$^{+/+}$/*p53*$^{-/-}$, *Bmi1*$^{+/-}$/*p53*$^{+/-}$, *Bmi1*$^{+/-}$/*p53*$^{+/+}$, *Bmi1*$^{-/-}$/*p53*$^{+/+}$ and *Bmi1*$^{-/-}$/*p53*$^{+/-}$ mice, but a single *Bmi1*$^{-/-}$/*p53*$^{-/-}$ mouse (expected n=12), for which size and viability did not improve. To evaluate the contribution of *p53* to the cone degeneration phenotype of *Bmi1*$^{-/-}$ mice, we performed double staining with S-opsin and peanut agglutinin (PNA), which labels the outer segments of all

Development (2016) 143, 1571-1584 doi:10.1242/dev.125351

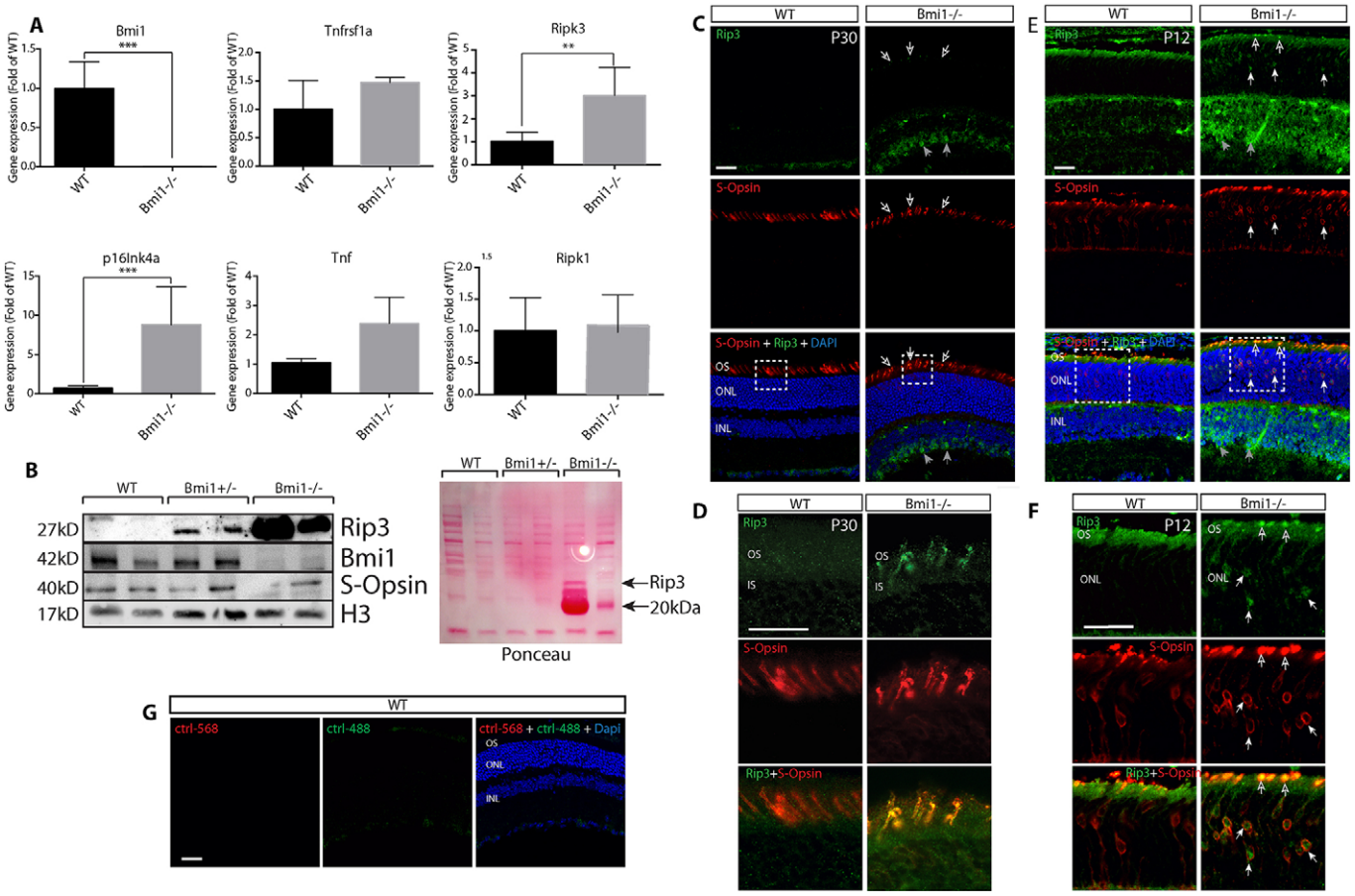

Fig. 5. Cone degeneration in *Bmi1*$^{-/-}$ mice operates through necroptosis. (A) RT-qPCR analysis of *Bmi1*$^{-/-}$ and WT retinal extracts at P30; *Bmi1* and *P16Ink4a* were used as internal controls. Values are expressed as fold of WT. (B) Western blot analyses of retinal extracts from WT, *Bmi1*$^{+/-}$ and *Bmi1*$^{-/-}$ mice. Note the gene dosage-dependent increase in Rip3 expression and the decrease in S-opsin expression in *Bmi1*$^{-/-}$ mice. Ponceau-red staining of the membrane is shown on the right. Histone H3 was used for protein normalization. (C-F) IF analyses on WT and *Bmi1*$^{-/-}$ retinas at P30 (C,D) and P12 (E,F). White-edged arrows, accumulation of Rip3 in S-cone outer segments; gray arrows, Rip3^{+} cells in the INL; white arrows, S-opsin^{+} cells with nuclear expression of Rip3 in *Bmi1*$^{-/-}$ mice at P12 not present at P30. (G) Control with secondary antibody only. INL, inner nuclear layer; ONL, outer nuclear layer; OS, outer segment; IS, inner segment. Scale bars: 40 µm. All values are means±s.e.m. $^{**}P\leq0.01$; $^{***}P\leq0.001$; Student's *t*-test.

cones. By confocal microscopy, we reconstructed retinal sections in 3D to calculate the number of cones and evaluate their morphology. Interestingly, while the number of S-opsin^{+}/PNA^{+} cells was reduced in *Bmi1*$^{-/-}$/*p53*$^{+/-}$ retinas when compared with WT, it was improved in the unique *Bmi1*$^{-/-}$/*p53*$^{-/-}$ retina sample (Fig. 7C,D). However, S-opsin labeling in the *Bmi1*$^{-/-}$/*p53*$^{-/-}$ retina remained fragmented and disorganized, suggesting improved survival, but not morphology, of S-cones (Fig. 7C). We also analyzed samples using the MitoSoxRed reagent, which reacts with mitochondrial ROS on unfixed tissue. In *Bmi1*$^{-/-}$/*p53*$^{+/-}$ retinal sections, we observed robust fluorescence when compared with WT, suggesting increased mitochondrial ROS. Notably, fluorescence was highly reduced in the *Bmi1*$^{-/-}$/*p53*$^{-/-}$ retina but was not completely restored to WT levels (Fig. 7E). These results revealed the partial contribution of *Chk2* and *p53* to the cone degeneration phenotype of *Bmi1*$^{-/-}$ mice.

BMI1 is enriched at heterochromatic foci in human cones

We previously reported *BMI1* expression in the human retina and its downregulation during aging (Abdouh et al., 2012). Here, we investigated localization of BMI1 in human photoreceptors. Using confocal IF analyses on adult human retinas, we observed punctuate BMI1 immunolabeling in the nucleus of photoreceptors (Fig. 8A-C). In some cells that co-labeled with S-opsin or M-opsin, BMI1 immunolabeling was even more robust and present as multiple foci per nucleus (Fig. 8A). To characterize the BMI1 immunolocalization pattern on the chromatin of cones, we performed dual immunolabeling with antibodies directed against distinct histone modifications. Although BMI1 did not colocalize with H3K9ac, it colocalized with H3K27me3 and H3K9me3, suggesting distribution at both facultative and constitutive heterochromatin in human cones (Fig. 8B).

BMI1 is required for human cone differentiation and chromatin integrity

To investigate the function of BMI1 during human cone development, we used a protocol allowing the differentiation of ~70% of human embryonic stem (hES) cells into cones (Zhou et al., 2015). This method results in the generation of immature S-cones expressing CRX (*CRX*), cone arrestin (*ARR3*) and S-opsin (*OPN1SW*) within 21 days (Fig. 9A,D,E). Importantly, *in vitro* generated S-cones expressed BMI1, which also colocalized with H3K9me3 (Fig. 9A,B). We infected hES cells with a lentivirus expressing a small hairpin RNA against *BMI1* (shBMI1) or scramble sequence (shScramble) and performed hygromycin selection for 10 days (Abdouh et al., 2009). The hES cells were

Development (2016) 143, 1571-1584 doi:10.1242/dev.125351

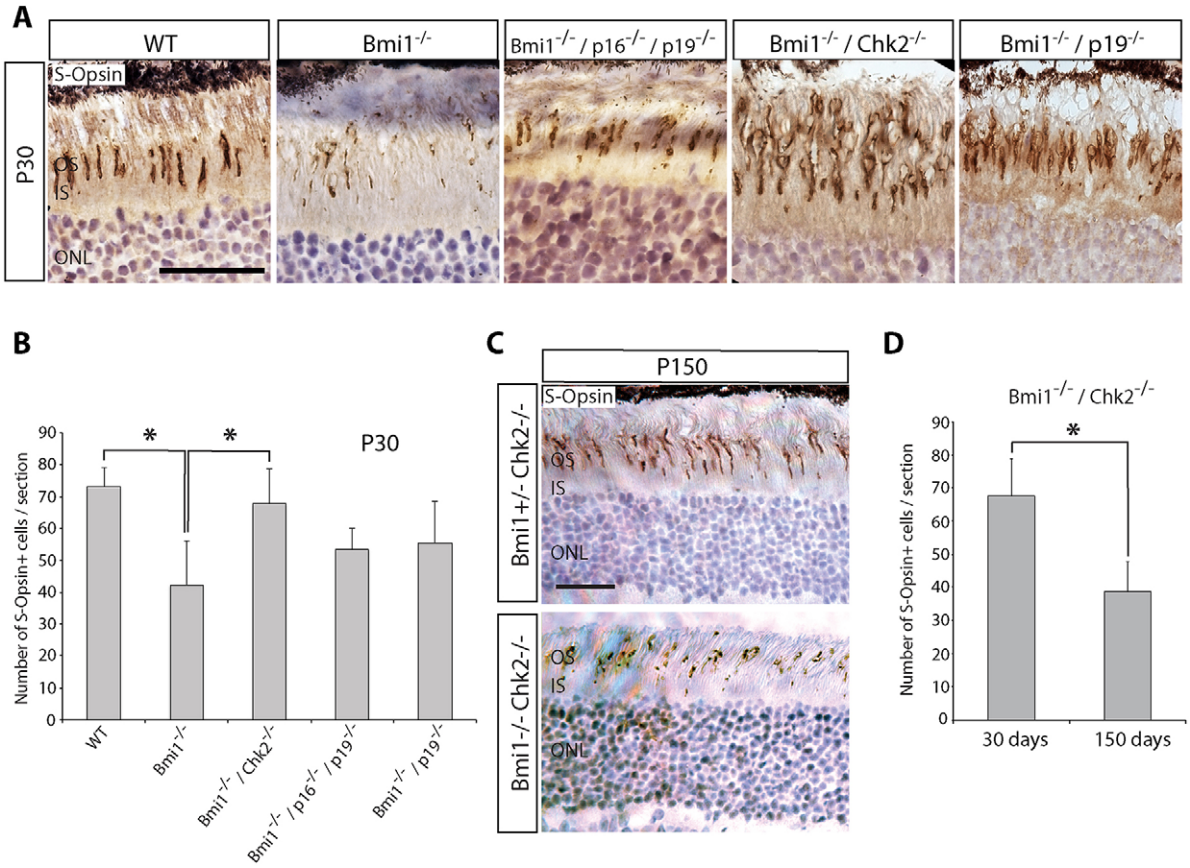

Fig. 6. *Chk2* genetic deficiency improves the *Bmi1*$^{-/-}$ cone degeneration phenotype. (A) Immunohistochemistry analyses of WT, *Bmi1*$^{-/-}$ and double mutant retinas at P30. (B) Quantification of the number of S-opsin^{+} photoreceptors per section for the five genotypes at P30 (n=4 mice for each genotype). (C) IHC analyses of retinas at P150. (D) Quantification of the number of S-opsin^{+} cells per field at P30 and P150. Scale bars: 40 µm. Quantifications are made from ×25 images. All values are means±s.e.m. *P≤0.05; Student's t-test.

then differentiated into S-cones for 21 days. Upon western blot analysis, BMI1 expression was hardly visible in naive hES cells, in contrast to *in vitro* differentiated cones (Fig. 9C). Histone H2Aub is the target of BMI1 and RING1a/b biochemical activity (Buchwald et al., 2006; Cao et al., 2005; Li et al., 2006; Wang et al., 2004). Consistently, histone H2Aub was reduced in differentiated cones upon knockdown of BMI1 (Fig. 9C). To confirm cone differentiation, we analyzed cells for expression of S-opsin and CRX (Chen et al., 1997; Freund et al., 1997, 1998; Furukawa et al., 1997, 1999). In control cells, S-opsin and CRX expression was observed in more than 70% of cells, as visualized by IF and western blot (Fig. 9A and D). By contrast, S-opsin and CRX expression was highly reduced in differentiated cones upon BMI1 knockdown (Fig. 9A,D). When using a hypomorphic construct against BMI1 that reduces BMI1 levels by ∼50% (shBMI1 50%) (Abdouh et al., 2009), CRX expression in differentiated cones was reduced by ∼25% when compared with levels in control cells, suggesting a modest gene-dosage effect (Fig. 9D). To consider the role of p53 activation in the context of *Bmi1* deficiency, we investigated p53 expression (Chatoo et al., 2009). Using an antibody against p53 that also recognizes other family members, i.e. p73 and p63, we observed predominant expression of p73 in shScramble and shBMI1 50% cones (Fig. 9D) (Jacobs et al., 2006). By contrast, p73 was lost in shBMI1 95% cones and was associated with induction of *p63* and *p53* (Fig. 9D). It was previously proposed that one main function of Polycomb group proteins in mouse ES cells is to prevent differentiation through repression of lineage-specific homeobox genes such as PAX, SOX and LHX families (Boyer et al., 2006). To further characterize the cone differentiation phenotype, we analyzed the hES cells by qPCR. We found that while the expression of cone-specific genes (*ARR3* and *OPN1SW*) and retinal homeobox genes (*RAX* and *SIX6*) was reduced by 50-75% in shBMI1 cells, expression of *SOX1* was increased by ∼6-fold when compared with control cells (Fig. 9E). *SOX1* and *SOX2* are enriched in neural stem cells and retinal progenitors but are not expressed in photoreceptors, thus providing a possible explanation for the defective terminal differentiation of cones upon knockdown of BMI1 (Avilion et al., 2003; Ellis et al., 2004; Graham et al., 2003; Taranova et al., 2006; Yan et al., 2005).

To investigate the effect of BMI1 knockdown on the chromatin of human cones, we performed IF analyses. BMI1 knockdown resulted in increased H3K9ac levels, but reduced H3K27me3 and H3K9me3 levels when compared with control cells (Fig. 9F). BMI1 knockdown was also associated with the formation of γH2Ax foci – a histone modification characteristic of DNA double-strand breaks and genomic instability (Fig. 9G) (Chagraoui et al., 2011; Facchino et al., 2010; Ismail et al., 2010; Rogakou et al., 1998). Consistent with the chromatin relaxation phenotype, we observed induction of repeat DNA sequences in BMI1 knockdown cones, with a modest gene-dosage effect when using the hypomorphic shBMI1 construct (Fig. 9H). These experiments revealed that BMI1 is required for terminal differentiation, heterochromatin compaction, silencing of repeat DNA and genomic stability in human cones.

Development (2016) 143, 1571-1584 doi:10.1242/dev.125351

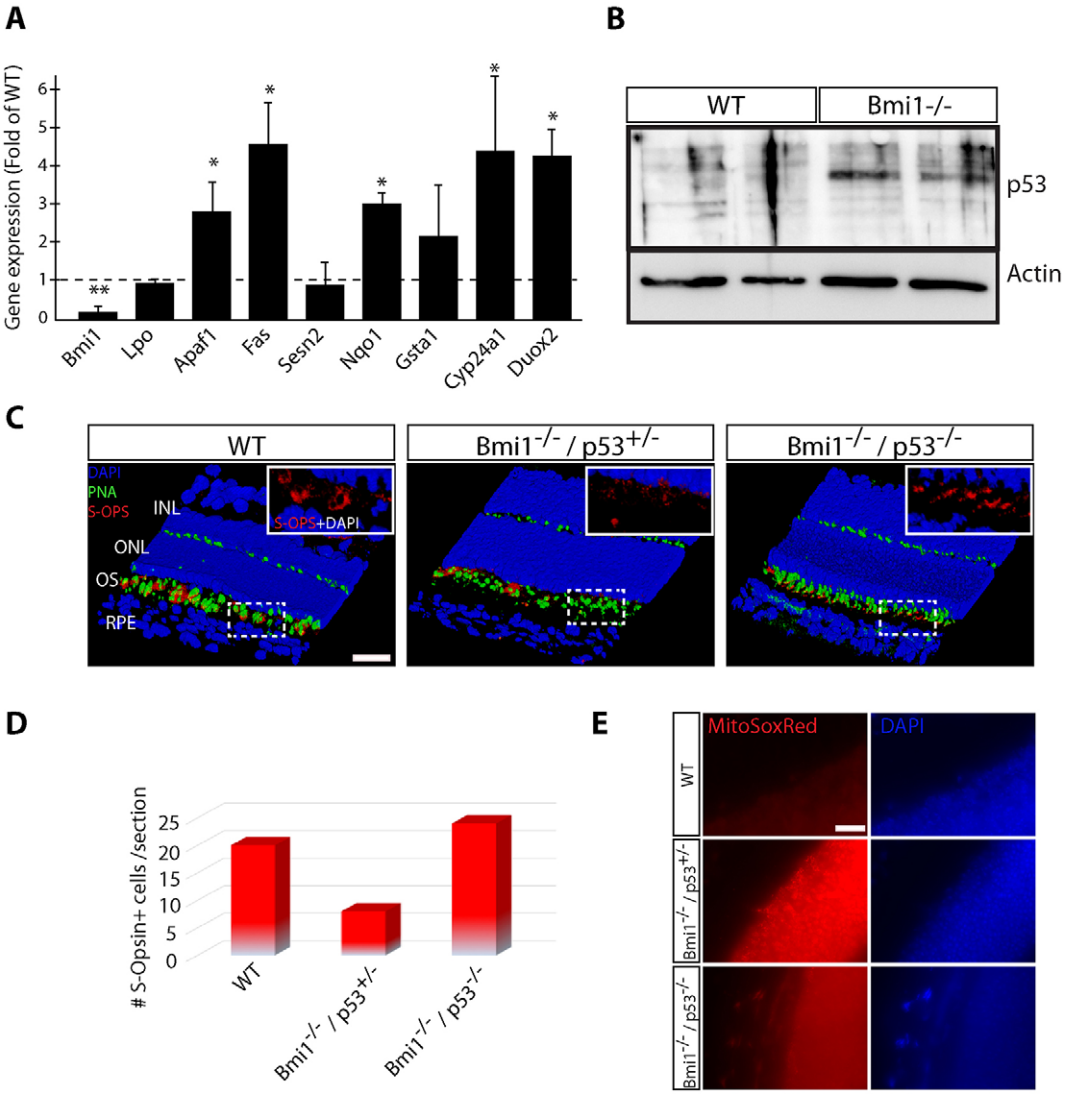

Fig. 7. *p53* genetic deficiency improves the *Bmi1*$^{-/-}$ cone degeneration phenotype. (A) Quantitative RT-PCR analysis of WT and *Bmi1*$^{-/-}$ retinal extracts at P30. *Bmi1* was used as negative control and all values are expressed as fold of WT. (B) Western blot analysis of mouse retinas at P30 showing p53 accumulation in *Bmi1* mutants. (C) 3D reconstruction by confocal microscopy analyses of WT, *Bmi1*$^{-/-}$/*p53*$^{+/-}$ and *Bmi1*$^{-/-}$/*p53*$^{-/-}$ retinas at P30. White box: detail of S-opsin in the outer segment in the dashed box. Note the lower immunoreactivity and the fragmentation of the S-opsin in *Bmi1*$^{-/-}$/*p53*$^{+/-}$ mice and a rescue in the quantity of S-opsin in the *Bmi1*$^{-/-}$/*p53*$^{-/-}$ even if it is still fragmented. (D) Quantification of S-opsin^{+} cells per section in WT, *Bmi1*$^{-/-}$/*p53*$^{+/-}$ and *Bmi1*$^{-/-}$/*p53*$^{-/-}$ mice. (E) IF analyses of WT and *Bmi1*$^{-/-}$ retinas at P30 stained with MitoSoxRed. Note the partial rescue in *Bmi1*$^{-/-}$/*p53*$^{-/-}$ mice when compared with WT. RPE, retinal pigment epithelium; ONL, outer nuclear layer; INL, inner nuclear layer; OS, outer segment. Scale bar: 50 µm in C; 20 µm in E. All values are means±s.e.m. *$P \leq 0.05$; **$P \leq 0.01$; Student's *t*-test.

DISCUSSION

We showed here that cone photoreceptors and bipolar neurons are normally generated but then undergo rapid degeneration in *Bmi1*$^{-/-}$ mice through Rip3-associated necroptosis. Selective retinal cell degeneration in *Bmi1*$^{-/-}$ mice also correlated with predominant Bmi1 expression in bipolar neurons and cone photoreceptors. Cone number but not morphology in *Bmi1*$^{-/-}$ mice was partially rescued by deletion of either *Chk2* or *p53*, implicating these additional pathways in neurodegeneration. BMI1 was expressed in human cones, where it localized at heterochromatic foci. BMI1 inactivation in hES cells severely perturbed differentiation of cones, in contrast to the situation found in *Bmi1*$^{-/-}$ mice. However, BMI1-deficient human cones also presented common features with the *Bmi1*$^{-/-}$ mouse retinal phenotype, thus revealing partially conserved functions across species.

In previous work, it was proposed that *Bmi1* inactivation could prevent rod and cone photoreceptor degeneration in *Rd1* mice, a model of retinitis pigmentosa (Zencak et al., 2013). *Rd1* mice carry a mutation in *Pde6b*, which is only expressed in rods. Thus, cone degeneration in *Rd1* mice is thought to be secondary to the loss of trophic support provided by rods. As apoptosis of rod photoreceptors in *Rd1* mice is preceded by cell cycle re-entry and activation of cyclin dependent kinases (CDKs), it was suggested that loss of *Bmi1* provides neuroprotection by blocking CDK activation and thus cell cycle re-entry of rods (Marigo, 2007; Sancho-Pelluz et al., 2008; Zencak et al., 2013). Here, we found that *Bmi1* deficiency was associated with the activation of several cell cycle inhibitors in the retina such as p16^{INK4a}, p19^{ARF}, Chk2 and p53, consistent with the general function of Bmi1 in inhibiting the p16^{INK4a}/CDK6/Rb and p19^{ARF}/p53/p21^{Cip1} pathways (Sauvageau and Sauvageau, 2010). Thus, taken in the context of the *Rd1*

Development (2016) 143, 1571-1584 doi:10.1242/dev.125351

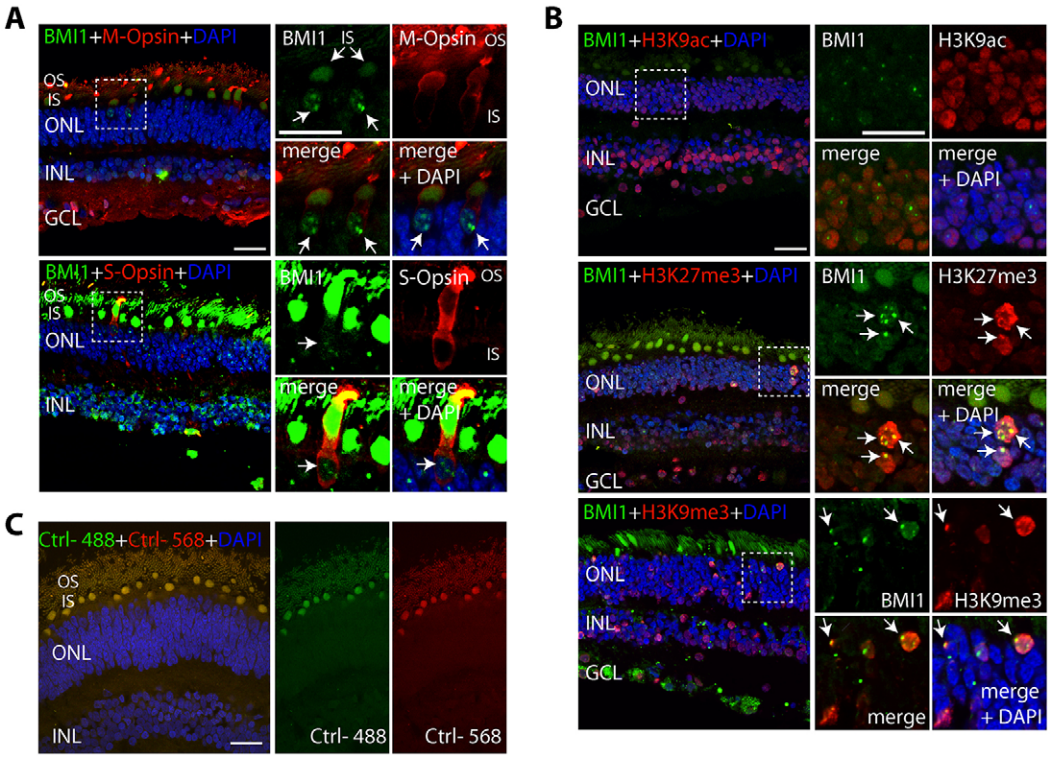

Fig. 8. BMI1 is enriched at heterochromatic nuclear foci in human cones. (A-C) Confocal IF analysis of BMI1 expression in the adult human retina. (A) BMI1 is expressed in the nucleus of M-opsin^{+} and S-opsin^{+} cones (arrows). (B) BMI1 is enriched at heterochromatic nuclear foci as shown by colocalization with H3K9me3 and H3K27me3 in cones (arrows). (C) Negative control with only the secondary antibody. Note the strong autofluorescence present in the IS and OS. ONL, outer nuclear layer; INL, inner nuclear layer; IS, inner segment; OS, outer segment; GCL, ganglion cell layer. Scale bars: 20 µm.

mutation, the proposed model is likely to be valid, but only in rods. Also, whether acute Bmi1 inhibition in *Rd1* mice can prevent rod degeneration remains to be demonstrated, as this would be more relevant to a clinical context. Interestingly, the outer segment of cones is abnormal in *Rd1*/*Bmi1*$^{-/-}$ mice, as shown using S-opsin immunolabeling, suggesting rod-independent cone degeneration (Zencak et al., 2013). This is consistent with our overall findings suggesting cell-autonomous degeneration of cones in *Bmi1*$^{-/-}$ mice.

Our genetic studies further revealed that *Chk2* or *p53* deletion could improve initial cone number in *Bmi1*$^{-/-}$ mice but not the outer segment morphology and progressive degeneration. This is consistent with previous work showing that in *Bmi1*$^{-/-}$ mice, *Chk2* inactivation improved several pathologies and lifespan, and that *p53* inactivation prevented cortical neuron cell death (Chatoo et al., 2009; Liu et al., 2009). However, the function of Bmi1 and p53 in the mouse retina, and especially in cones, are apparently not identical as in cortical neurons. For example, although p53-dependent apoptotic cell death was predominant in *Bmi1*$^{-/-}$ cortical neurons, it was not in *Bmi1*$^{-/-}$ cones, where we observed Rip3-associated necroptosis. At the molecular level, expression of the phase II antioxidant genes *Nqo1* and *Gsta1* was also not reduced in *Bmi1*$^{-/-}$ retinas, in contrast to *Bmi1*$^{-/-}$ cortices. Because these are direct p53 targets, this suggests that p53 activity is distinct between the retina and brain in the context of *Bmi1* deficiency.

In recent years, necroptosis was revealed as an alternative mechanism of cell death in many pathological contexts (Linkermann and Green, 2014; Vandenabeele et al., 2010). In the retina, it was found that cones, not rods, are especially vulnerable to necroptosis. For example, mutation in the cone-specific gene *PDE6C* results in achromaptosis, a disease characterized by cone degeneration (Chang et al., 2009). Using a zebrafish mutant for *pde6c*, it was shown that cone degeneration is mediated by rip1 and rip3, and that inhibition of necroptosis with necrostatin-1 can delay the disease process. Interestingly, necroptosis also operates in cones even when cone cell death is non cell-autonomous, such as in *rd10* mice carrying a mutation in the rod-specific gene *pde6b* (Murakami et al., 2012). Here again, treatment of *rd10* mice with necrostatin-1 greatly improved the cone degeneration phenotype, bringing hope for a possible pharmaceutical treatment of cone degenerative diseases.

Using directed differentiation of hES cells as model of retinal development, we demonstrated that BMI1 is required for the terminal differentiation of human cones. By contrast, expression of retinal homeobox genes and of *Opn1sw* was not altered in *Bmi1*$^{-/-}$ mouse retinas, revealing possible inter-species differences. These differences might, however, be explained by compensation mechanisms operating during development in *Bmi1*$^{-/-}$ mice but not in *BMI1* knockdown cells or by the highly distinct experimental systems. For example, acute *Bmi1* inactivation in embryonic mouse cortical progenitors was shown to induce massive apoptosis, in sharp contrast to the situation observed in *Bmi1*$^{-/-}$ mice (Fasano et al., 2007). Taken in a broader context, it is interesting to note that mice conditionally deficient for *Ezh2*, the catalytic subunit of the PRC2, which tri-methylates histone H3 at lysine 27, show reduced RPC proliferation and increased apoptosis, but not post natal degeneration of retinal neurons (Zhang et al., 2015). Likewise, mice deficient for *G9a* (*Ehmt2*), which di-methylates histone H3 at lysine 9, show increased RPC apoptosis and persistent cell proliferation (Katoh et al., 2012). In both cases, inefficient repression of non-retinal genes such as *Six1* (*Ezh2* knockout) or RPC genes such as *Hes1*, *Chx10* and *Lhx2* (*G9a* knockout) perturbs the terminal differentiation of retinal cells. These two situations are thus similar

Development (2016) 143, 1571-1584 doi:10.1242/dev.125351

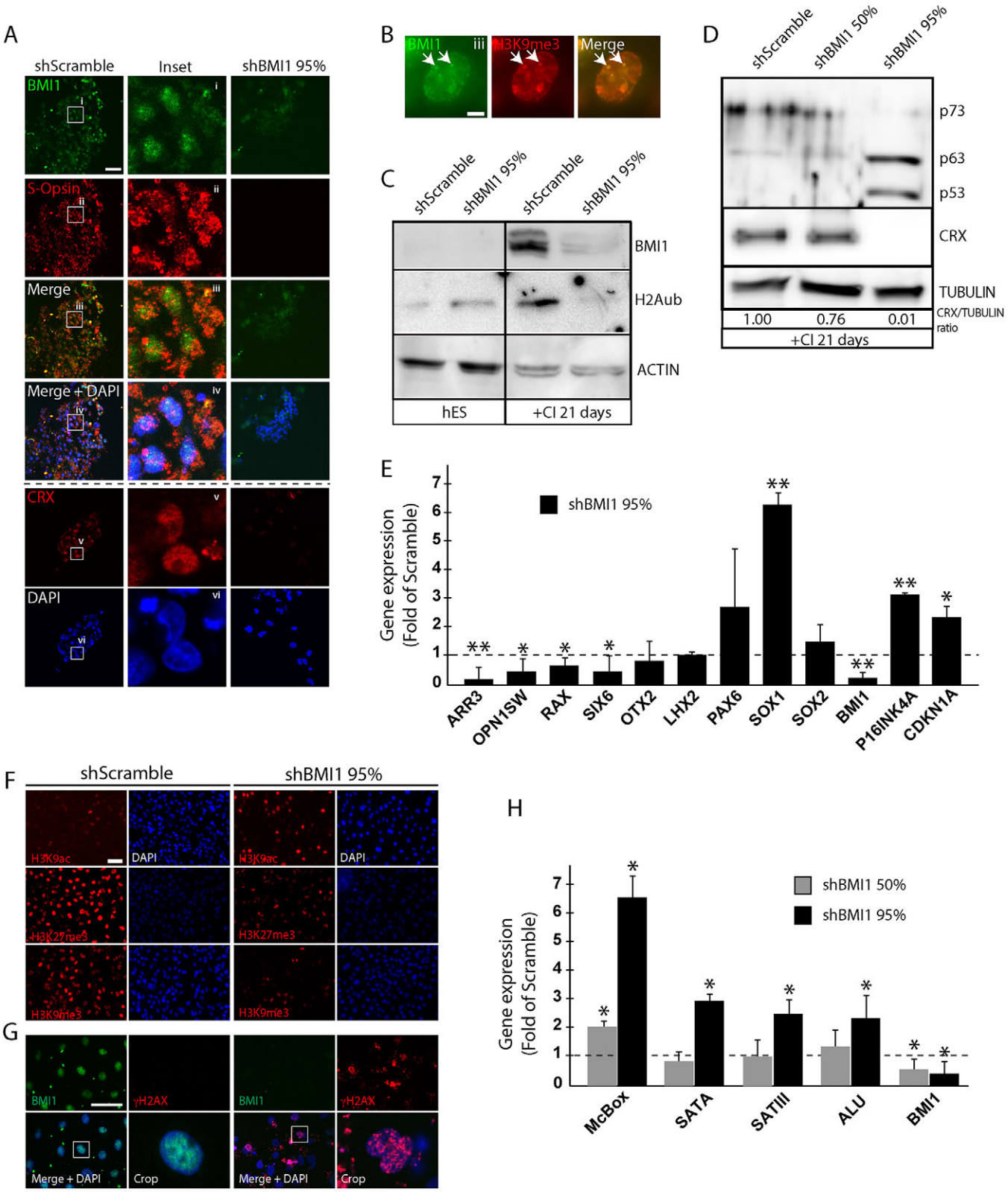

Fig. 9. BMI1 is required for terminal differentiation, heterochromatin compaction and genomic stability of human cones. (A,B) IF analysis of hES cells differentiated for 21 days toward the cone photoreceptor cell lineage. (A) In controls (shSrcamble), BMI1 is expressed in the nucleus of S-opsin^{+} cells. In shBMI1 cells, BMI1, S-opsin and CRX expression were highly reduced when compared with controls. (B) Colocalization of BMI1 and H3K9me3 in cones (arrows). (C,D) Western blot analyses of hES cells and *in vitro* differentiated cones (+CI 21 days) infected with shScramble or shBMI1 viruses. Note that BMI1 knockdown affects histone H2Aub levels only in cones; BMI1 knockdown in human cones was accompanied by induction of *p53*. Quantification of CRX levels normalized to tubulin; note the dose-dependent reduction in CRX expression in BMI1 knockdown cells. (E,H) Quantitative RT-PCR analyses of *in vitro* differentiated cones for retinal markers (E) and repeat DNA sequences (H). BMI1 was used as negative control and values are expressed as fold of Scramble value. (F,G) IF analyses of hES cell-derived cones (day 21). Scale bars: 20 µm in A,F,G; 2 µm in B. All values are means±s.e.m. *P≤0.05; **P≤0.01; Student's *t*-test.

Development (2016) 143, 1571-1584 doi:10.1242/dev.125351

to what we have observed in BMI1 deficient cones, where expression of *SOX1* was abnormally upregulated. At the level of the chromatin, it was demonstrated that rod photoreceptors of mice deficient for all three linker histone H1 genes have reduced chromatin condensation and increased nuclear diameter (Popova et al., 2013), a phenotype similar to that found in *Bmi1*$^{-/-}$ mouse photoreceptors and BMI1-deficient human cones. The results suggesting that BMI1 functions to prevent heterochromatin loss and expression of tandem repeats in photoreceptors are also novel findings. Since constitutive heterochromatin is the most instable portion of the mammalian genome (Bhaskara et al., 2010; Kappes et al., 2011; Larson et al., 2012; Peng and Karpen, 2009; Rowe et al., 2010), this could explain part of the genomic instability phenotype observed in BMI1 deficient cells (Chagraoui et al., 2011; Facchino et al., 2010; Ismail et al., 2010).

In conclusion, we demonstrated that Bmi1 expression in the retina is not required for retinal cell type genesis but is important to prevent bipolar neuron and cone photoreceptor degeneration during post natal development. Retinal cell death in *Bmi1*$^{-/-}$ mice was mediated by the activity of Chk2 and p53 on the one hand, and by Rip3-associated necroptosis on the other. Whether necroptosis is directly repressed by Bmi1 or indirectly mediated by the activity of p53 or Chk2 remains to be elucidated. Using an *in vitro* model of human cone development, we further demonstrated that BMI1 is required for the terminal differentiation of cones and maintenance of their genomic integrity. Further experiments, through inactivation of BMI1 in terminally differentiated cones, should address whether BMI1 is important to prevent human cone photoreceptor degeneration and/or maintenance of cell type identity.

MATERIALS AND METHODS

Mice and human tissues

Mice knockout for *p53*, *p16*^{INK4a} or *p16*^{INK4a}/*p19*^{ARF} were obtained from the Jackson Laboratory. Wild-type mice from the C57BL/6 genetic background were obtained from Charles River, Saint-Constant, Canada. Fresh human eyes were provided by the eye bank of Maisonneuve-Rosemont Hospital.

The Animal Care Committee of the Maisonneuve-Rosemont Hospital Research Centre approved the use of the animals in this study. Post mortem human eyes were provided by the Banque d'yeux du Québec du Centre Michel-Mathieu (http://www.maisonneuve-rosemont.org/pages/h/hopital/HMRCentreMichelMathieu.aspx) and were used with approbation of the Comité d'Éthique à la Recherche de l'Hôpital Maisonneuve-Rosemont. Human embryonic stem cells were used in accordance to Canadian Institute Health Research (CIHR) guidelines and approved by the Comité de Surveillance de la Recherche sur les Cellules Souches (CSRCS) of the CIHR.

Cell culture

The hES cell line H9 (WiCell) was cultured on BD matrigel-coated plate (BD bioscience) with a daily change of mTeSR medium according to the manufacturer's instructions (STEMCELL Technologies) (Thomson et al., 1998). The H9 hES cell line was first established on mouse embryonic fibroblasts (MEFs) and then cultured on Matrigel in mTeSR medium. For derivation of S-cones, undifferentiated hES cell colonies expanded at near confluence were cultured in DMEM-F12 medium supplemented with 2% B27, 1% N2, 1% NEAM (Life Technologies), 10 ng/ml IGF-1, 10 ng/ml FGF2 (Peprotech), 10 mg/ml heparin (Sigma) and 30 ng/ml Coco (R&D Systems) for 21 days. Retinal cells were cultured from eyes of WT and knockout mice as described in detail in supplementary Materials and Methods.

ERG recording and analysis

Electroretinograms (ERGs) were recorded on mice (WT, n=4; *Bmi1*$^{+/-}$, n=3; *Bmi1*$^{-/-}$, n=3) in photopic and scotopic conditions to assess the cone and rod systems activity, respectively, according to a previously described procedure (Lavoie et al., 2014). Detailed information is available in supplementary Materials and Methods.

Immunohistochemistry and immunofluorescence

Tissues were fixed by immersion in 4% paraformaldehyde (PFA)/3% sucrose in PBS, pH 7.4 for 1 h at room temperature. Samples were washed three times in PBS, cryoprotected in PBS/30% sucrose and frozen in Ctyomatrix embedding medium (CEM) (Thermo Shandon) or in Tissue-Tek optimum cutting temperature (O.C.T.) compound (Sakura Finetek). Otherwise, tissues were fixed in 10% buffered formalin and embedded in paraffin according to standard protocols. 5- to 12-µm-thick sections were mounted on Super-Frost glass slides (Fisher Scientific) and processed for immunofluorescence or immunohistochemistry staining. Detailed information on the experimental procedure and antibodies used is available in supplementary Materials and Methods.

Retinal dissection and eye orientation

Eyes were labeled in the dorsal pole of the cornea by puncturing with a needle tip. Eyes were extracted, fixed in 4% PFA overnight and stored in PBS. The retinas were marked by a small incision following the respective mark on the cornea. Retinas were then dissected as flattened whole mounts by four radial cuts and processed for IF using standard procedures, as describe above. Retinas were mounted between two coverslips that were attached to a slide by scotch tape, allowing flip-flopping of the retinas for analysis by microscope. For preparation of the blocks for cryosectioning, eyes were marked as described above, and oriented in blocks to maintain the eye polarity.

Quantification of retinal cell types

To collect sections from the ventral retina, blocks were trimmed up to the optic nerve and sections collected. For quantification, three successive images were taken on the nasal side from a set distance from the optic nerve. At least three different mice were used for each genotype (1 eye per animal), except for the *p53*$^{-/-}$/*Bmi1*$^{-/-}$ mouse where only two eyes were available. Positive cells were counted manually using ImageJ software (NIH). For IF analysis, single analysis of green channel (488) and red channel (568) were done to prevent filter overlap. To assess the general distribution of cones, whole mounts were photographed with a 10× objective using a Zeiss microscope (Observer.Z1) equipped with computer-driven motorized stage (VEXTA stepping motor), and individual frames were tiled to reconstruct the whole mounts (about 36 images/retina) using AxioVision 4.8 software. For quantification of IF images, photos were taken with a confocal microscope equipped with a 60× objective. Three images were taken per sample, where n=4 eyes per condition, at the same distance from the optic nerve in the naso-ventral portion of the retina. Photoreceptors labeled with PNA or with S-opsin and PNA were counted manually using ImageJ software. Quantifications of IHC experiments were performed in the same way but using images taken with a Zeiss microscope (Observer.Z1) equipped with a 25× objective.

Quantitative RT-PCR

All primers were designed to flank individual exons and tested by PCR in RT+ and RT− control extracts. Total RNA was isolated using TRIzol reagent (Invitrogen). Reverse transcription (RT) was performed using 1 µg total RNA and the MML-V reverse transcriptase (Invitrogen). Quantitative real-time PCR (qPCR) was performed using the Platinum SYBR Green SuperMix (Invitrogen) and a real-time PCR apparatus (ABI Prism 7000). GAPDH was used as an internal standard for data calibration. The $2^{-\Delta\Delta Ct}$ formula was used for the calculation of differential gene expression. All experiments were performed at least in triplicate. Primer sequences are available in supplementary Materials and Methods. Primer sets for repetitive sequences were as described previously (Zhu et al., 2011).

Lentiviral infection

The shRNA-expressing lentiviral plasmids were cotransfected with plasmids pCMVdR8.9 and pHCMVG into 293FT packaging cells using

Development (2016) 143, 1571-1584 doi:10.1242/dev.125351

Lipofectamine (Invitrogen) according to the manufacturer's instructions. Virus-containing media were collected, filtered and concentrated by ultracentrifugation. Viral titers were measured by serial dilution on 293T cells followed by microscopic analysis 48 h later. For viral transduction, lentiviral vectors were added to dissociated cells before plating. Hygromycin selection (150 µg/ml) was started 48 h later.

Western blot

Western blots of WT and *Bmi1* mutant mouse retinas were carried out using standard procedures with antibodies listed in supplementary Materials and Methods.

Statistical analyses

Statistical differences were analyzed using the Student's *t*-test for unpaired samples with equal s.d. using two-tailed *P*-value. For ERG experiments, analysis of variance were made by one-way ANOVA followed by Bonferroni's multiple comparisons test. For photoreceptor quantification in flat mount retinas, the analysis of variance was performed by two-way ANOVA followed by Tukey's multiple comparison test with 95% confidence. Data are presented as means±s.d. Values are representative of at least three experiments. The criterion for significance (*P*-value) was set as reported in the figures.

Acknowledgements

We thank M. Van Lohuizen for the *Bmi1*$^{+/-}$ mice and A. Swaroop for the *Nrl*$^{-/-}$ mouse eyes.

Competing interests

The authors declare no competing or financial interests.

Author contributions

Performed the experiments: A.B., V.P., M.A., W.C., A.F., R.H., S.Z. and J.L. Designed the experiments and wrote the manuscript: G.B., A.B., A.F., J.L. and M.H. Provided materials: N.M.

Funding

This work was supported by grants from the Natural Science and Engineering Research Council of Canada (NSERC); Antoine-Turmel Foundation for Macular Degeneration Research; and the Foundation Fighting Blindness Canada. V.P. was supported by a fellowship from NSERC. A.F. was supported by fellowships from Montreal University Molecular Biology Program and Réseau Vision du Québec.

Supplementary information

Supplementary information available online at
http://dev.biologists.org/lookup/suppl/doi:10.1242/dev.125351/-/DC1

References

Abdouh, M., Facchino, S., Chatoo, W., Balasingam, V., Ferreira, J. and Bernier, G. (2009). BMI1 sustains human glioblastoma multiforme stem cell renewal. *J. Neurosci.* **29**, 8884-8896.

Abdouh, M., Chatoo, W., El Hajjar, J., David, J., Ferreira, J. and Bernier, G. (2012). Bmi1 is down-regulated in the aging brain and displays antioxidant and protective activities in neurons. *PLoS ONE* **7**, e31870.

Avilion, A. A., Nicolis, S. K., Pevny, L. H., Perez, L., Vivian, N. and Lovell-Badge, R. (2003). Multipotent cell lineages in early mouse development depend on SOX2 function. *Genes Dev.* **17**, 126-140.

Belecky-Adams, T., Cook, B. and Adler, R. (1996). Correlations between terminal mitosis and differentiated fate of retinal precursor cells in vivo and in vitro: analysis with the "window-labeling" technique. *Dev. Biol.* **178**, 304-315.

Bernier, G., Panitz, F., Zhou, X., Hollemann, T., Gruss, P. and Pieler, T. (2000). Expanded retina territory by midbrain transformation upon overexpression of Six6 (Optx2) in Xenopus embryos. *Mech. Dev.* **93**, 59-69.

Bhaskara, S., Knutson, S. K., Jiang, G., Chandrasekharan, M. B., Wilson, A. J., Zheng, S., Yenamandra, A., Locke, K., Yuan, J.-L., Bonine-Summers, A. R. et al. (2010). Hdac3 is essential for the maintenance of chromatin structure and genome stability. *Cancer Cell* **18**, 436-447.

Boyer, L. A., Plath, K., Zeitlinger, J., Brambrink, T., Medeiros, L. A., Lee, T. I., Levine, S. S., Wernig, M., Tajonar, A., Ray, M. K. et al. (2006). Polycomb complexes repress developmental regulators in murine embryonic stem cells. *Nature* **441**, 349-353.

Buchwald, G., van der Stoop, P., Weichenrieder, O., Perrakis, A., van Lohuizen, M. and Sixma, T. K. (2006). Structure and E3-ligase activity of the Ring–Ring complex of polycomb proteins Bmi1 and Ring1b. *EMBO J.* **25**, 2465-2474.

Cao, R., Tsukada, Y.-i. and Zhang, Y. (2005). Role of Bmi-1 and Ring1A in H2A ubiquitylation and Hox gene silencing. *Mol. Cell* **20**, 845-854.

Carl, M., Loosli, F. and Wittbrodt, J. (2002). Six3 inactivation reveals its essential role for the formation and patterning of the vertebrate eye. *Development* **129**, 4057-4063.

Cepko, C. L., Austin, C. P., Yang, X., Alexiades, M. and Ezzeddine, D. (1996). Cell fate determination in the vertebrate retina. *Proc. Natl. Acad. Sci. USA* **93**, 589-595.

Chagraoui, J., Hebert, J., Girard, S. and Sauvageau, G. (2011). An anticlastogenic function for the Polycomb Group gene Bmi1. *Proc. Natl. Acad. Sci. USA* **108**, 5284-5289.

Chang, B., Grau, T., Dangel, S., Hurd, R., Jurklies, B., Sener, E. C., Andreasson, S., Dollfus, H., Baumann, B., Bolz, S. et al. (2009). A homologous genetic basis of the murine Cpfl1 mutant and human achromatopsia linked to mutations in the PDE6C gene. *Proc. Natl. Acad. Sci. USA* **106**, 19581-19586.

Chatoo, W., Abdouh, M., David, J., Champagne, M.-P., Ferreira, J., Rodier, F. and Bernier, G. (2009). The polycomb group gene Bmi1 regulates antioxidant defenses in neurons by repressing p53 pro-oxidant activity. *J. Neurosci.* **29**, 529-542.

Chatoo, W., Abdouh, M., Duparc, R.-H. and Bernier, G. (2010). Bmi1 distinguishes immature retinal progenitor/stem cells from the main progenitor cell population and is required for normal retinal development. *Stem Cells* **28**, 1412-1423.

Chatoo, W., Abdouh, M. and Bernier, G. (2011). P53 pro-oxidant activity in the central nervous system: implication in aging and neurodegenerative diseases. *Antioxid. Redox Signal.* **15**, 1729-1737.

Chen, S., Wang, Q.-L., Nie, Z., Sun, H., Lennon, G., Copeland, N. G., Gilbert, D. J., Jenkins, N. A. and Zack, D. J. (1997). Crx, a novel Otx-like paired-homeodomain protein, binds to and transactivates photoreceptor cell-specific genes. *Neuron* **19**, 1017-1030.

Chow, R. L., Altmann, C. R., Lang, R. A. and Hemmati-Brivanlou, A. (1999). Pax6 induces ectopic eyes in a vertebrate. *Development* **126**, 4213-4222.

Ellis, P., Fagan, B. M., Magness, S. T., Hutton, S., Taranova, O., Hayashi, S., McMahon, A., Rao, M. and Pevny, L. (2004). SOX2, a persistent marker for multipotential neural stem cells derived from embryonic stem cells, the embryo or the adult. *Dev. Neurosci.* **26**, 148-165.

Facchino, S., Abdouh, M., Chatoo, W. and Bernier, G. (2010). BMI1 confers radioresistance to normal and cancerous neural stem cells through recruitment of the DNA damage response machinery. *J. Neurosci.* **30**, 10096-10111.

Fasano, C. A., Dimos, J. T., Ivanova, N. B., Lowry, N., Lemischka, I. R. and Temple, S. (2007). shRNA knockdown of Bmi-1 reveals a critical role for p21-Rb pathway in NSC self-renewal during development. *Cell Stem Cell* **1**, 87-99.

Fodor, B. D., Shukeir, N., Reuter, G. and Jenuwein, T. (2010). Mammalian Su(var) genes in chromatin control. *Annu. Rev. Cell Dev. Biol.* **26**, 471-501.

Fortin, A., Cregan, S. P., MacLaurin, J. G., Kushwaha, N., Hickman, E. S., Thompson, C. S., Hakim, A., Albert, P. R., Cecconi, F., Helin, K. et al. (2001). APAF1 is a key transcriptional target for p53 in the regulation of neuronal cell death. *J. Cell Biol.* **155**, 207-216.

Freund, C. L., Gregory-Evans, C. Y., Furukawa, T., Papaioannou, M., Looser, J., Ploder, L., Bellingham, J., Ng, D., Herbrick, J.-A. S., Duncan, A. et al. (1997). Cone-rod dystrophy due to mutations in a novel photoreceptor-specific homeobox gene (CRX) essential for maintenance of the photoreceptor. *Cell* **91**, 543-553.

Freund, C. L., Wang, Q.-L., Chen, S., Muskat, B. L., Wiles, C. D., Sheffield, V. C., Jacobson, S. G., McInnes, R. R., Zack, D. J. and Stone, E. M. (1998). De novo mutations in the CRX homeobox gene associated with Leber congenital amaurosis. *Nat. Genet.* **18**, 311-312.

Furukawa, T., Morrow, E. M. and Cepko, C. L. (1997). Crx, a novel otx-like homeobox gene, shows photoreceptor-specific expression and regulates photoreceptor differentiation. *Cell* **91**, 531-541.

Furukawa, T., Morrow, E. M., Li, T., Davis, F. C. and Cepko, C. L. (1999). Retinopathy and attenuated circadian entrainment in Crx-deficient mice. *Nat. Genet.* **23**, 466-470.

Graham, V., Khudyakov, J., Ellis, P. and Pevny, L. (2003). Sox2 functions to maintain neural progenitor identity. *Neuron* **39**, 749-765.

Haverkamp, S. and Wässle, H. (2000). Immunocytochemical analysis of the mouse retina. *J. Comp. Neurol.* **424**, 1-23.

Hennig, A. K., Peng, G.-H. and Chen, S. (2013). Transcription coactivators p300 and CBP are necessary for photoreceptor-specific chromatin organization and gene expression. *PLoS ONE* **8**, e69721.

Ismail, I. H., Andrin, C., McDonald, D. and Hendzel, M. J. (2010). BMI1-mediated histone ubiquitylation promotes DNA double-strand break repair. *J. Cell Biol.* **191**, 45-60.

Jacobs, J. J., Kieboom, K., Marino, S., DePinho, R. A. and van Lohuizen, M. (1999). The oncogene and Polycomb-group gene bmi-1 regulates cell proliferation and senescence through the ink4a locus. *Nature* **397**, 164-168.

Jacobs, W. B., Kaplan, D. R. and Miller, F. D. (2006). The p53 family in nervous system development and disease. *J. Neurochem.* **97**, 1571-1584.

Jadhav, A. P., Mason, H. A. and Cepko, C. L. (2006). Notch 1 inhibits photoreceptor production in the developing mammalian retina. *Development* **133**, 913-923.

Development (2016) 143, 1571-1584 doi:10.1242/dev.125351

Jia, L., Oh, E. C., Ng, L., Srinivas, M., Brooks, M., Swaroop, A. and Forrest, D. (2009). Retinoid-related orphan nuclear receptor RORbeta is an early-acting factor in rod photoreceptor development. *Proc. Natl. Acad. Sci. USA* **106**, 17534-17539.

Kappes, F., Waldmann, T., Mathew, V., Yu, J., Zhang, L., Khodadoust, M. S., Chinnaiyan, A. M., Luger, K., Erhardt, S., Schneider, R. et al. (2011). The DEK oncoprotein is a Su(var) that is essential to heterochromatin integrity. *Genes Dev.* **25**, 673-678.

Karimi, M. M., Goyal, P., Maksakova, I. A., Bilenky, M., Leung, D., Tang, J. X., Shinkai, Y., Mager, D. L., Jones, S., Hirst, M. et al. (2011). DNA methylation and SETDB1/H3K9me3 regulate predominantly distinct sets of genes, retroelements, and chimeric transcripts in mESCs. *Cell Stem Cell* **8**, 676-687.

Katoh, K., Yamazaki, R., Onishi, A., Sanuki, R. and Furukawa, T. (2012). G9a histone methyltransferase activity in retinal progenitors is essential for proper differentiation and survival of mouse retinal cells. *J. Neurosci.* **32**, 17658-17670.

Lagutin, O. V., Zhu, C. C., Kobayashi, D., Topczewski, J., Shimamura, K., Puelles, L., Russell, H. R. C., McKinnon, P. J., Solnica-Krezel, L. and Oliver, G. (2003). Six3 repression of Wnt signaling in the anterior neuroectoderm is essential for vertebrate forebrain development. *Genes Dev.* **17**, 368-379.

Larson, K., Yan, S. J., Tsurumi, A., Liu, J., Zhou, J., Gaur, K., Guo, D., Eickbush, T. H. and Li, W. X. (2012). Heterochromatin formation promotes longevity and represses ribosomal RNA synthesis. *PLoS Genet.* **8**, e1002473.

Lavoie, J., Illiano, P., Sotnikova, T. D., Gainetdinov, R. R., Beaulieu, J. M. and Hebert, M. (2014). The electroretinogram as a biomarker of central dopamine and serotonin: potential relevance to psychiatric disorders. *Biol. Psychiatry* **75**, 479-486.

Li, Z., Cao, R., Wang, M., Myers, M. P., Zhang, Y. and Xu, R.-M. (2006). Structure of a Bmi-1-Ring1B polycomb group ubiquitin ligase complex. *J. Biol. Chem.* **281**, 20643-20649.

Linkermann, A. and Green, D. R. (2014). Necroptosis. *N. Engl. J. Med.* **370**, 455-465.

Liu, J., Cao, L., Chen, J., Song, S., Lee, I. H., Quijano, C., Liu, H., Keyvanfar, K., Chen, H., Cao, L.-Y. et al. (2009). Bmi1 regulates mitochondrial function and the DNA damage response pathway. *Nature* **459**, 387-392.

Loosli, F., Winkler, S. and Wittbrodt, J. (1999). Six3 overexpression initiates the formation of ectopic retina. *Genes Dev.* **13**, 649-654.

Marigo, V. (2007). Programmed cell death in retinal degeneration: targeting apoptosis in photoreceptors as potential therapy for retinal degeneration. *Cell Cycle* **6**, 652-655.

Marquardt, T. (2003). Transcriptional control of neuronal diversification in the retina. *Prog. Retin. Eye Res.* **22**, 567-577.

Marquardt, T., Ashery-Padan, R., Andrejewski, N., Scardigli, R., Guillemot, F. and Gruss, P. (2001). Pax6 is required for the multipotent state of retinal progenitor cells. *Cell* **105**, 43-55.

Mathers, P. H., Grinberg, A., Mahon, K. A. and Jamrich, M. (1997). The Rx homeobox gene is essential for vertebrate eye development. *Nature* **387**, 603-607.

Mears, A. J., Kondo, M., Swain, K. S., Takada, Y., Bush, R. A., Saunders, T. L., Sieving, P. A. and Swaroop, A. (2001). Nrl is required for rod photoreceptor development. *Nat. Genet.* **29**, 447-452.

Molofsky, A. V., He, S., Bydon, M., Morrison, S. J. and Pardal, R. (2005). Bmi-1 promotes neural stem cell self-renewal and neural development but not mouse growth and survival by repressing the p16Ink4a and p19Arf senescence pathways. *Genes Dev.* **19**, 1432-1437.

Murakami, Y., Matsumoto, H., Roh, M., Suzuki, J., Hisatomi, T., Ikeda, Y., Miller, J. W. and Vavvas, D. G. (2012). Receptor interacting protein kinase mediates necrotic cone but not rod cell death in a mouse model of inherited degeneration. *Proc. Natl. Acad. Sci. USA* **109**, 14598-14603.

Ng, L., Hurley, J. B., Dierks, B., Srinivas, M., Saltó, C., Vennström, B., Reh, T. A. and Forrest, D. (2001). A thyroid hormone receptor that is required for the development of green cone photoreceptors. *Nat. Genet.* **27**, 94-98.

Nishida, A., Furukawa, A., Koike, C., Tano, Y., Aizawa, S., Matsuo, I. and Furukawa, T. (2003). Otx2 homeobox gene controls retinal photoreceptor cell fate and pineal gland development. *Nat. Neurosci.* **6**, 1255-1263.

Ortín-Martínez, A., Nadal-Nicolás, F. M., Jiménez-López, M., Alburquerque-Béjar, J. J., Nieto-López, L., García-Ayuso, D., Villegas-Pérez, M. P., Vidal-Sanz, M. and Agudo-Barriuso, M. (2014). Number and distribution of mouse retinal cone photoreceptors: differences between an albino (Swiss) and a pigmented (C57/BL6) strain. *PLoS ONE* **9**, e102392.

Peng, J. C. and Karpen, G. H. (2009). Heterochromatic genome stability requires regulators of histone H3 K9 methylation. *PLoS Genet.* **5**, e1000435.

Popova, E. Y., Grigoryev, S. A., Fan, Y., Skoultchi, A. I., Zhang, S. S. and Barnstable, C. J. (2013). Developmentally regulated linker histone H1c promotes heterochromatin condensation and mediates structural integrity of rod photoreceptors in mouse retina. *J. Biol. Chem.* **288**, 17895-17907.

Porter, F. D., Drago, J., Xu, Y., Cheema, S. S., Wassif, C., Huang, S. P., Lee, E., Grinberg, A., Massalas, J. S., Bodine, D. et al. (1997). Lhx2, a LIM homeobox gene, is required for eye, forebrain, and definitive erythrocyte development. *Development* **124**, 2935-2944.

Reh, T. A. and Kljavin, I. J. (1989). Age of differentiation determines rat retinal germinal cell phenotype: induction of differentiation by dissociation. *J. Neurosci.* **9**, 4179-4189.

Rogakou, E. P., Pilch, D. R., Orr, A. H., Ivanova, V. S. and Bonner, W. M. (1998). DNA double-stranded breaks induce histone H2AX phosphorylation on serine 139. *J. Biol. Chem.* **273**, 5858-5868.

Rowe, H. M., Jakobsson, J., Mesnard, D., Rougemont, J., Reynard, S., Aktas, T., Maillard, P. V., Layard-Liesching, H., Verp, S., Marquis, J. et al. (2010). KAP1 controls endogenous retroviruses in embryonic stem cells. *Nature* **463**, 237-240.

Sancho-Pelluz, J., Arango-Gonzalez, B., Kustermann, S., Romero, F. J., van Veen, T., Zrenner, E., Ekström, P. and Paquet-Durand, F. (2008). Photoreceptor cell death mechanisms in inherited retinal degeneration. *Mol. Neurobiol.* **38**, 253-269.

Sauvageau, M. and Sauvageau, G. (2010). Polycomb group proteins: multi-faceted regulators of somatic stem cells and cancer. *Cell Stem Cell* **7**, 299-313.

Sharpless, N. E., Ramsey, M. R., Balasubramanian, P., Castrillon, D. H. and DePinho, R. A. (2004). The differential impact of p16(INK4a) or p19(ARF) deficiency on cell growth and tumorigenesis. *Oncogene* **23**, 379-385.

Sherr, C. J. (2001). The INK4a/ARF network in tumour suppression. *Nat. Rev. Mol. Cell Biol.* **2**, 731-737.

Solovei, I., Kreysing, M., Lanctôt, C., Kösem, S., Peichl, L., Cremer, T., Guck, J. and Joffe, B. (2009). Nuclear architecture of rod photoreceptor cells adapts to vision in mammalian evolution. *Cell* **137**, 356-368.

Swaroop, A., Wang, Q.-L., Wu, W., Cook, J., Coats, C., Xu, S., Chen, S., Zack, D. J. and Sieving, P. A. (1999). Leber congenital amaurosis caused by a homozygous mutation (R90W) in the homeodomain of the retinal transcription factor CRX: direct evidence for the involvement of CRX in the development of photoreceptor function. *Hum. Mol. Genet.* **8**, 299-305.

Swaroop, A., Kim, D. and Forrest, D. (2010). Transcriptional regulation of photoreceptor development and homeostasis in the mammalian retina. *Nat. Rev. Neurosci.* **11**, 563-576.

Taranova, O. V., Magness, S. T., Fagan, B. M., Wu, Y., Surzenko, N., Hutton, S. R. and Pevny, L. H. (2006). SOX2 is a dose-dependent regulator of retinal neural progenitor competence. *Genes Dev.* **20**, 1187-1202.

Thomson, J. A., Itskovitz-Eldor, J., Shapiro, S. S., Waknitz, M. A., Swiergiel, J. J., Marshall, V. S. and Jones, J. M. (1998). Embryonic stem cell lines derived from human blastocysts. *Science* **282**, 1145-1147.

Valk-Lingbeek, M. E., Bruggeman, S. W. M. and van Lohuizen, M. (2004). Stem cells and cancer; the polycomb connection. *Cell* **118**, 409-418.

van der Lugt, N. M., Domen, J., Linders, K., van Roon, M., Robanus-Maandag, E., te Riele, H., van der Valk, M., Deschamps, J., Sofroniew, M., van Lohuizen, M. et al. (1994). Posterior transformation, neurological abnormalities, and severe hematopoietic defects in mice with a targeted deletion of the bmi-1 proto-oncogene. *Genes Dev.* **8**, 757-769.

Vandenabeele, P., Galluzzi, L., Vanden Berghe, T. and Kroemer, G. (2010). Molecular mechanisms of necroptosis: an ordered cellular explosion. *Nat. Rev. Mol. Cell Biol.* **11**, 700-714.

Viringipurampeer, I. A., Shan, X., Gregory-Evans, K., Zhang, J. P., Mohammadi, Z. and Gregory-Evans, C. Y. (2014). Rip3 knockdown rescues photoreceptor cell death in blind pde6c zebrafish. *Cell Death Differ.* **21**, 665-675.

Wang, H., Wang, L., Erdjument-Bromage, H., Vidal, M., Tempst, P., Jones, R. S. and Zhang, Y. (2004). Role of histone H2A ubiquitination in Polycomb silencing. *Nature* **431**, 873-878.

Watanabe, T. and Raff, M. C. (1990). Rod photoreceptor development in vitro: intrinsic properties of proliferating neuroepithelial cells change as development proceeds in the rat retina. *Neuron* **4**, 461-467.

Yan, Y., Yang, D., Zarnowska, E. D., Du, Z., Werbel, B., Valliere, C., Pearce, R. A., Thomson, J. A. and Zhang, S.-C. (2005). Directed differentiation of dopaminergic neuronal subtypes from human embryonic stem cells. *Stem Cells* **23**, 781-790.

Yanagi, Y., Takezawa, S. and Kato, S. (2002). Distinct functions of photoreceptor cell-specific nuclear receptor, thyroid hormone receptor beta2 and CRX in one photoreceptor development. *Invest. Ophthalmol. Vis. Sci.* **43**, 3489-3494.

Yaron, O., Farhy, C., Marquardt, T., Applebury, M. and Ashery-Padan, R. (2006). Notch1 functions to suppress cone-photoreceptor fate specification in the developing mouse retina. *Development* **133**, 1367-1378.

Zencak, D., Schouwey, K., Chen, D., Ekstrom, P., Tanger, E., Bremner, R., van Lohuizen, M. and Arsenijevic, Y. (2013). Retinal degeneration depends on Bmi1 function and reactivation of cell cycle proteins. *Proc. Natl. Acad. Sci. USA* **110**, E593-E601.

Zhang, J., Taylor, R. J., La Torre, A., Wilken, M. S., Cox, K. E., Reh, T. A. and Vetter, M. L. (2015). Ezh2 maintains retinal progenitor proliferation, transcriptional integrity, and the timing of late differentiation. *Dev. Biol.* **403**, 128-138.

Zhou, S., Flamier, A., Abdouh, M., Tetreault, N., Barabino, A., Wadhwa, S. and Bernier, G. (2015). Differentiation of human embryonic stem cells into cone photoreceptors through simultaneous inhibition of BMP, TGFbeta and Wnt signaling. *Development* **142**, 3294-3306.

Zhu, Q., Pao, G. M., Huynh, A. M., Suh, H., Tonnu, N., Nederlof, P. M., Gage, F. H. and Verma, I. M. (2011). BRCA1 tumour suppression occurs via heterochromatin-mediated silencing. *Nature* **477**, 179-184.

SUPPLEMENTARY MATERIALS AND METHODS

ERG recording and analysis

A typical ERG trace is composed of the a-wave, which is a negative component originating from the photoreceptors, and the b-wave, which is a positive component generated by the bipolar and Müller cells complex stimulation. Two major parameters can be derived from these waves, namely the amplitude (μV) and the implicit time (ms). By convention, the amplitude of the a-wave is measured from the baseline to trough, and the b-wave amplitude is measured from the trough of the a-wave to the peak of the b-wave. The implicit time of the waves represents the number of milliseconds at which the maximal amplitude is reached. For each of the four parameters, a photopic and scotopic luminance response function (LRF) was generated, where the values of the parameters were plotted against flash luminance. Repeated measures analyses of variance with Bonferroni correction were performed to assess the difference between the three genotypes for each one of the parameters. All analyses were conducted using SPSS for Windows, version 22.0.

Immunohistochemistry and immunofluorescence

For immunofluorescence labeling, sections were incubated overnight with primary antibody solutions at 4ºC in a humidified chamber. After three washes in PBS, sections were incubated with secondary antibodies for 1 h at room temperature. Slides were mounted on coverslips in DAPI-containing mounting medium (Vector Laboratories, CA). For immunohistochemistry labeling, slices were analyzed by using the Vectastain® ABC kit (Vector) according to the manufacturer instructions. Peroxidase substrates used are the Vector® VIP (Pink) (Vector), and DAB (brown) (Sigma). Observations were made under a fluorescence microscope (Leica DMRE, Leica Microsystems) and images were captured with a digital camera (Retiga EX; QIMAGING; with OpenLab, ver.3.1.1 software; Open-Lab, Canada). Confocal microscopy analyses were performed using 60x objectives with an IX81 confocal microscope (Olympus, Richmond Hill, Canada), and images were obtained with Fluoview software version 3.1 (Olympus). 3D reconstructions were obtained with Fluoview software version 3.1 from 18-25 z-stack image. Primary antibodies used in this study are: sheep anti-Chx10 (1:250, Exalpha Biologicals), rabbit anti-Pax6 (1:500, Chemicon), mouse anti-Bmi1 (1:200, US Biological), rabbit anti-Bmi1 (1:150, US Biological), mouse anti-Syntaxin (1:200, Sigma), mouse anti-4D2 (Rhodopsin) (1:100, R. Molday, UBC), mouse anti-Gad65 (1:300, BD Pharmingen), rabbit anti-CORD2 (CRX) (1:300, Abcam), rabbit anti-S-Opsin (1:200, Invitrogen), rabbit anti-M-Opsin (1:100, Chemicon), Rip3 (1:250, Santa Cruz), rabbit anti-H3K9me3 (1:500, Abcam), rabbit anti-H3K9ac (1:300, Cell Signaling), rabbit anti-H3K27me3 (1:300, Cell Signaling), mouse anti-glutamine synthetase (GS) (1:100, Chemicon), rabbit anti-Pkcα

(1:500, Sigma), rabbit anti-Calbidin (1:500, Chemicon), rabbit anti-Recoverin (1:1000, Millipore), mouse anti-γH2Ax (1:250, Millipore), rabbit anti-Cralbp (1:500, kindly given by Dr Saari's lab). Secondary antibodies are: donkey AlexaFluor488-conjugated anti-mouse (1:1000, Life Technologies), donkey AlexaFluor488-conjugated anti-rabbit (1:1000, Life Technologies), goat AlexaFluor594-conjugated anti-mouse IgM (1:1000, Invitrogen), donkey AlexaFluor633-conjugated anti-sheep (1:1000, Molecular Probes), goat AlexaFluor647-conjugated anti-mouse (1:1000, Life Technologies) goat AlexaFluor texas red-conjugated anti-rabbit (1:1000, Life Technologies), donkey FITC-conjugated anti-mouse (1:300, Chemicon), goat FITC-conjugated anti-rat (1:300, Caltag Laboratories), donkey Rhodamine-conjugated anti-rabbit (1:300, Chemicon). Fluorescein labeled Peanut Agglutinin (PNA) (1:200, Vector laboratories) was used to stain the outer segment of PRs. Superoxide production was measured by red fluorescence intensity as described by standard protocol indicated by manufacturer (MitoSoxRed mitochondrial superoxide indicator, Molecular Probes, U.S.).

Quantitative RT-PCR

Mouse primer sets used are:

Tnf (F) 5' AAAATTCGAGTGACAAGCCTGTAG 3'; Tnf (R) 5' CCCTTGAAGAGAACCTGGGAGTAG 3'; Tnfrsf1a (F) 5' GCCGGATATGGGCATGAAGC 3'; Tnfrsf1a (R) 5' TGTCTCAGCCCTCACTTGAC 3'; Ripk1 (F) 5' TGTCATCTAGCGGGAGGTTG 3'; Ripk1 (R) 5' TCACCACTCGACTGTGTCTCAG 3'; Ripk3 (F) 5' CTCCGTGCCTTGACCTACTG 3'; Ripk3 (R) 5' AACCATAGCCTTCACCTCCC3'; Bmi1 (F) 5'-GGAGACCAGCAAGTATTGTCCTATTTG-3', Bmi1 (R) 5'-CTTACGATGCCCAGCAGCAATG-3'; $p16^{Ink4a}$ (F) 5'-CAACGCCCCGAACTCTTTC-3', $p16^{Ink4a}$ (R) 5'-GCAGAAGAGCTGCTACGTGAAC-3'; $p19^{Arf}$ (F) 5'-GGCTAGAGAGGATCTTGAGAAGAGG-3', $p19^{Arf}$ (R) 5'-GCCCATCATCATCACCTGGTCCAGG-3'; Sox2 (F) 5'-TAAGGGTTCTTGCTGGGTTTT-3', Sox2 (R) 5'-AGACCACGAAAACGGTCTTG-3'; Lhx2 (F) 5'-GATCTCGCCTGGAAACAGAG -3', Lhx2 (R) 5'-TCGCTCAGTCCACAAAACTG -3'; Otx2 (F) 5'-AGAGGAGGTGGCACTGAAAA-3', Otx2 (R) 5'-TGACCTCCATTCTGCTGTTG-3'; Lpo (F) 5'-AGGTCTGTTGGCCAAGAATG-3', Lpo (R) 5'-ATGTTGATGGAAGCCAGGTC-3'; Apaf1 (F) 5'-TGCTCAGCGGATAAGAAGGT-3', Apaf1 (R) 5'TCCCAGAGCTTGAGGAAGAA-3'; Fas (F) 5'-AAACAAACTGCACCCTGACC-3', Fas (R) 5'CAACCATAGGCGATTTCTGG-3'; Nqo1 (F) 5'-TTCTCTGGCCGATTCAGAGT-3', Nqo1 (R) 5'GAGTGTGGCCAATGCTGTAA-3'; Gsta1 (F) 5'-CGCCACCAAATATGACCTCT-3', Gsta1 (R) 5'CCATGGCTCTTCAACACCTT-3';

Cyp24a1 (F) 5'-GGCGGAAGATGTGAGGAATA-3', Cyp24a1 (R) 5'GTTGTGAATGGCACACTTGG-3'; Duox2 (F) 5'-ACAAGGGGTGTATGCCTTTG-3', Duox2 (R) 5'-CACAGGTTGTGGTAGCGAAA-3'. Crx (F) 5'-CCTTCTGACAGCTCGGTGTT-3', Crx (R) 5'-CCACTTTCTGAAGCCTGGAG)-3'; Sesn2 (F) 5'-CCTCCTTTGTGTTGTGCTGT-3', Sesn2 (R) 5'-ACGGTTCTCCATTTCCTCCT-3'; Opn1sw (F) 5'-CAGCCTTCATGGGATTTGTCT-3', Opn1sw (R) 5'-CAAAGAGGAAGTATCCGTGAC-3'; Rax (F) 5′-TGGGCTTTACCAAGGAAGACG-3', Rax (R) 5′-GGTAGCAGGGCCTAGTAGCTT-3'; Six6 (F) 5′-GCAAGTAGCCGGGGTATGTG-3', Six6 (R) 5′-CGACTCATTCTTGTTAAGGGCTT-3'; Nrl (F) 5′-CCCAGTCCCTTGGCTATGGA-3', Nrl (R) 5′-ACCGAGCTGTATGGTGTGGA-3'; Notch1 (F) 5′-GATGGCCTCAATGGGTACAAG-3', Notch1 (R) 5′-TCGTTGTTGTTGATGTCACAGT-3'; Pax6 (F) 5′-TGGCAAACAACCTGCCTATG-3', Pax6 (R) 5′-TGCACGAGTATGAGGAGGTCT-3'; Gapdh (F) 5′-AGGTCGGTGTGAACGGATTTG-3′, Gapdh (R) 5′-TGTAGACCATGTAGTTGAGGTCA-3';

Human primer sets used are:

PAX6 (F) 5'-AGATTTCAGAGCCCCATATTCG-3', PAX6 (R) 5'-CCATTTGGCCCTTCGATTAG-3'; ARR3 (F) 5'-CCCAGAGCTTTGCAGTAACC-3', ARR3 (R) 5'-CACAGGACACCATCAGGTTG-3'; SOX1 (F) 5'-AAAGTCAAAACGAGGCGAGA-3', SOX1 (R) 5'-AAGTGCTTGGACCTGCCTTA-3'; RAX (F) 5'-GGCAAGGTCAACCTACCAGA-3', RAX (R) 5'-GCTTCATGGAGGACACTTCC-3'; SIX6 (F) 5′- ACAGACTCCAGCAGCAGGTT-3′, SIX6 (R) 5′-AGATGTCGCACTCACTGTCG-3′; OPN1SW (F) 5′-TGTGCCTCTCTCCCTCATCT-3′, OPN1SW (R) 5′-GGCACGTAGCAGACACAGAA-3′; $p16^{INK4A}$ (F) 5′-GATCCAGGTGGGTAGAAGGTC-3′, $p16^{INK4A}$ (R) 5′-CCCCTGCAAACTTCGTCCT-3′; CDKN1A (F) 5′-CCGAAGTCAGTTCCTTGTGG-3′, CDKN1A (R) 5′-GTCGAAGTTCCATCGCTCAC3′; SOX2 (F) 5′-CACAACTCGGAGATCAGCAA-3′, SOX2 (R) 5′-CGGGGCCGGTATTTATAATC-3′; LHX2 (F) 5′-CCAAGGACTTGAAGCAGCTC-3′, LHX2 (R) 5′-TAAGAGGTTGCGCCTGAACT-3′; BMI1 (F) 5-AATCCCCACCTGATGTGTGT-3, BMI1 (R) 5-GCTGGTCTCCAGGTA ACGAA-3; GAPDH (F) 5-TCACCAGGGCTGCTTTTAAC-3′, GAPDH (R) 5′-ATCCACAGTCTTCTGGGTGG -3′.

Western blot

Total protein extracts were prepared in the Complete Mini protease inhibitor cocktail solution (Roche Diagnostics). Proteins contents were quantified using the Bradford reagent. Proteins were

resolved in Laemmli buffer by SDS-PAGE and transferred to a 0.2µm Nitrocellulose Blotting Membrane (BioRad) that was exposed to the primary antibodies: mouse anti-Bmi1 (1:800, Millipore), mouse anti-H2Aub (1:1000, Millipore), mouse anti- βActin (1:1000, abcam), p63, mouse anti-p73 (1:500, abcam), mouse anti-p53 (1:500, Santa Cruz Biotecnology), goat anti-CRX (1:500, Santa Cruz Biotecnology), mouse anti-α-Tubulin (1:1000, Sigma), anti-Rip3 (1:1000, Santa Cruz Biotecnology), anti-Bmi1 (1:500, abgent), S-Opsin (1:400, Santa Cruz Biotechnology) and histone H3 (1:1000, upstate). Membranes were treated with corresponding horseradish peroxidase-conjugated secondary antibodies (Sigma) and developed using the Immobilon Western (Millipore).

Cell cultures

Cultures of retinal cells were obtained by dissecting the mice eyes at P5 in 1X oxygenated HBSS (Life Technologies) in order to extract only the neural retina. Retinal cells were then re-suspended and incubated 10 minutes at 37 °C in the enzyme solution composed of 10ml 1X HBSS, 9.3 mg of Papain (Worthington), 1.6 mg of N-acetyl L-cysteine (Sigma), 0.5 mg of DNaseI (Roche) and 10µl EDTA 500mM (Fisher Scientific). After centrifugation cells were dissociated into Neurobasal^{tm} medium (Life technologies) with 0.02 µg/µl NGF (Invitrogen), 0.02 µg/µl BDNF (Invitrogen), 1% B27 (Invitrogen), 70 µg/ml gentamycin (Invitrogen), 1% fetal bovine serum (Wisent), 0.5% glucose (Sigma) and 10 µM Forskolin (Sigma). The cells were then spread and cultivated on coverslips treated with Poly-L-Lysine hydrobromide (Sigma) and BD Matrigel Matrix (BD Biosciences).

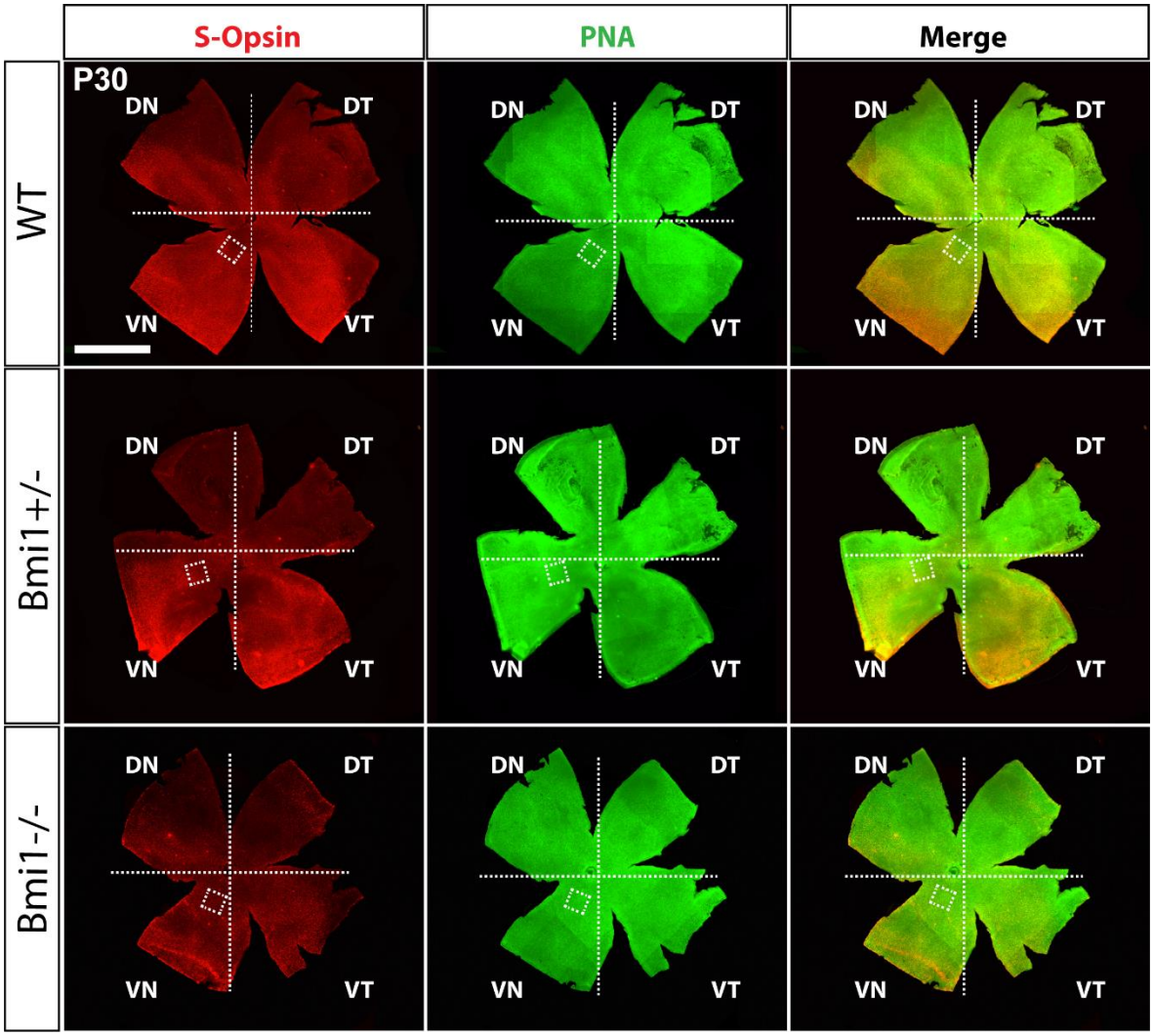

Figure S1. *Bmi1* is required for cone photoreceptor maintenance after birth

(A) Representative images from S-Opsin/PNA double-stained retinal flat mounts from WT, *Bmi1*$^{+/-}$ and *Bmi1*$^{-/-}$ mice at P30. Dorso-nasal (DN), dorso-temporal (DT), ventro-nasal (VN), ventro-temporal (VT). Scale bars: 1 mm.

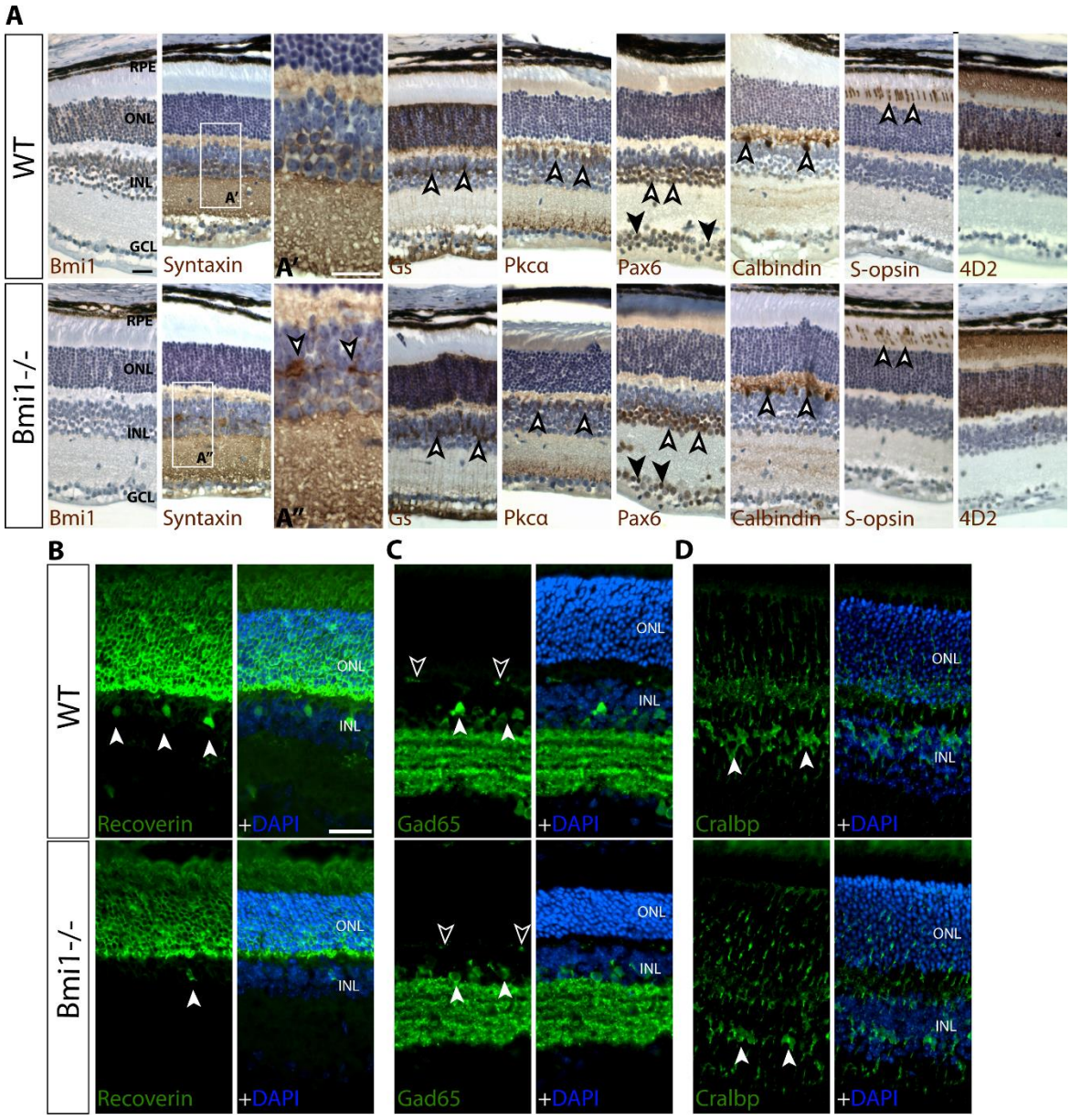

Figure S2. Histological anomalies in *Bmi1*$^{-/-}$ mouse retinas

(A, B, C, D) IHC and IF analyses of WT and *Bmi1*$^{-/-}$ retinas at P30 using specific markers for different retinal cell types. (A', A'') crop of the area indicated by the respective dashed rectangles. Amacrine cells' membrane (Syntaxin), müller glial cells (Gs and Cralbp), rods bipolar cells (Pkcα), amacrine (white-edged arrows) and ganglion cells (black arrows) (Pax6), horizontal cells (Calbindin), c-cones (S-Opsin), rod photoreceptors (4D2), T2 OFF and T8 ON cone bipolar cells (Recoverin), amacrine cells (white arrows) and horizontal cells (white-edged arrows) (Gad65). Retinal pigmented epithelium (RPE); outer nuclear layer (ONL); inner nuclear layer (INL); and ganglion cell layer (GCL). Scale bars: 40μm.

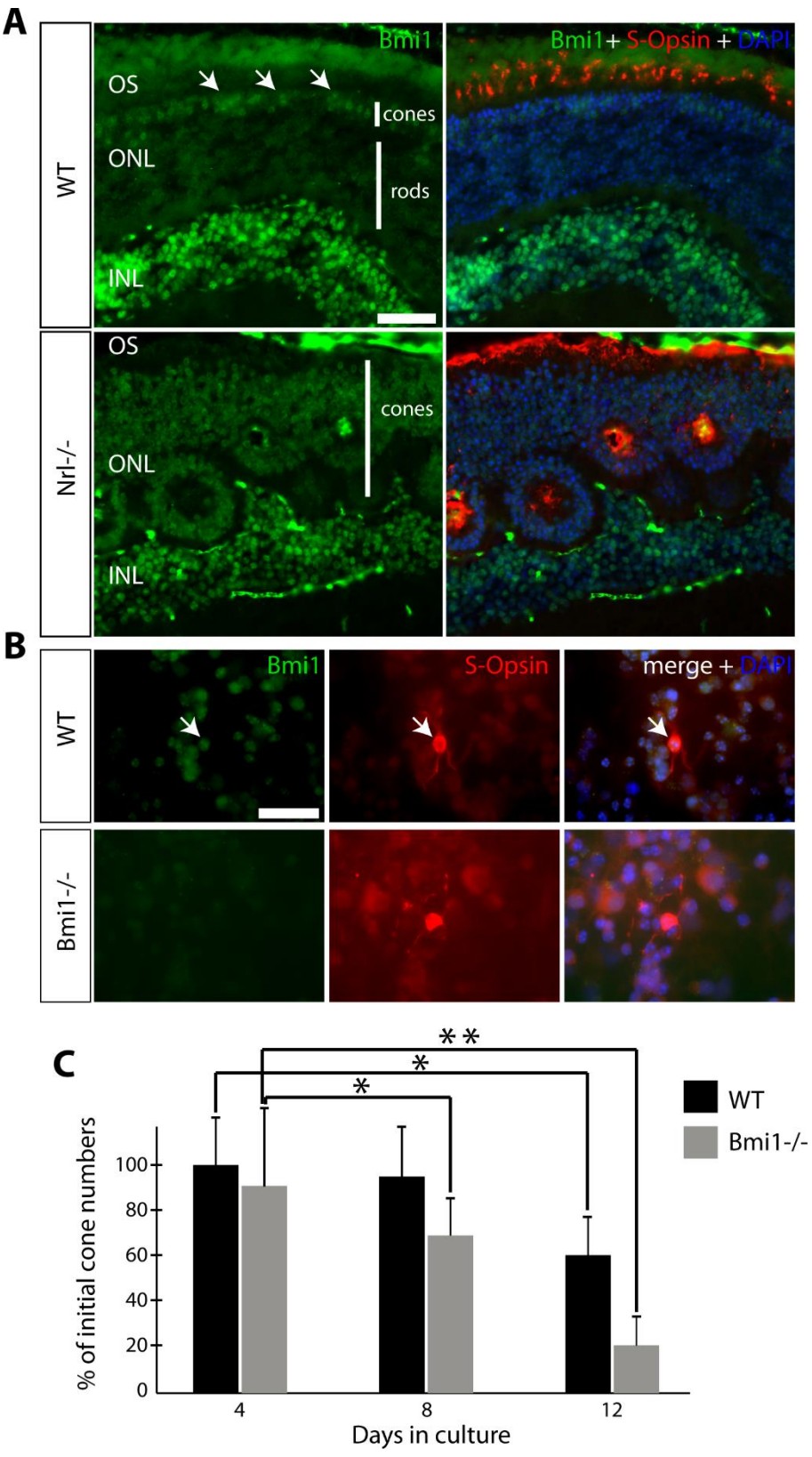

Figure S3. Bmi1 is preferentially expressed in mouse cone photoreceptors

(A) IF analysis of WT and *Nrl*$^{-/-}$ mouse retinal cryosections at P30. Arrows: Note the preferential expression of Bmi1 in neurons of the INL and in cone photoreceptors located in the ONL (white arrows). In contrast, Bmi1 is evenly distributed in the cone-only ONL of *Nrl*$^{-/-}$ mice. (B) IF analysis

of dissociated retinal cultures from WT and *Bmi1*$^{-/-}$ mice at P1 after 4 days *in vitro* (DIV). Note the expression of Bmi1 in WT cones labeled with S-Opsin, and the absence of Bmi1 in S-Opsin positive cells of *Bmi1*-mutants. (C) Quantification of S-Opsin positive cones in dissociated WT and *Bmi1*$^{-/-}$ retinal cultures, expressed as percentage of the initial cone number evaluated at 1 DIV. Outer nuclear layer (ONL); inner nuclear layer (INL); outer segment (OS). Scale bar: 50µm (A) and 20µm (B). WT n=4; *Bmi1*$^{-/-}$ n= 5. All values are mean ±SEM. (*) $P \leq 0.05$; (**) ≤ 0.01; Student t-test.

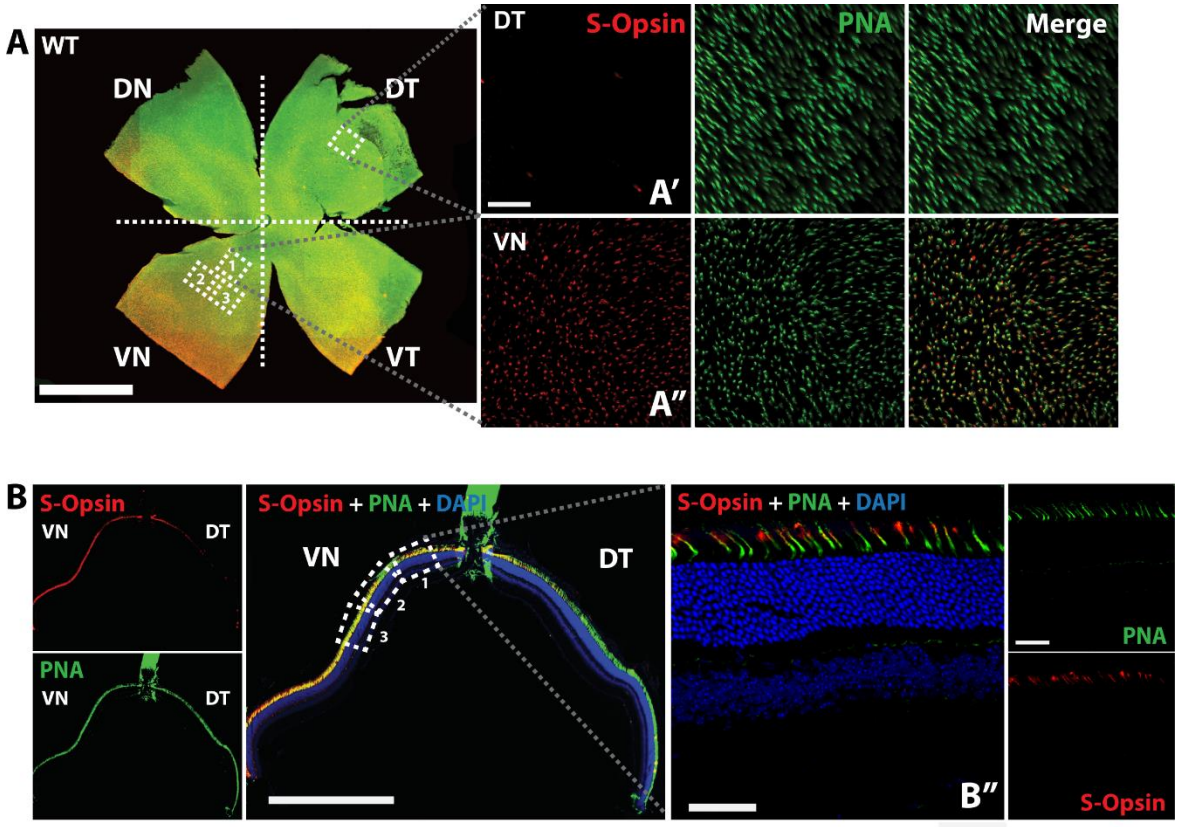

Figure S4. Methodology for the quantification of photoreceptors and other retinal cells types

(A) Representative mosaic reconstruction from 10x images from S-Opsin/PNA double-stained retinal flat mounts from P30 WT mice. (A', A'') 60x confocal microscopy images from retinal flat mount of the DT (A') and from the VN (A'') portion indicate with dashed rectangles in (A). (A') Note the almost complete absence of S-cone (S-Opsin+ cells) in the DT portion where almost only M-pure cones are present. (A") Note that in the VN portion approximately all cones express S-Opsin. The majority of these are dual-photoreceptors expressing both S and M Opsin and a minority of pure S-cone (data not shown). For PRs quantification, 3 images from the VN portion were quantified and averaged as shown by the dashed rectangles in (A). (B) 20x Mosaic Image of the whole retinal section at the level of the optic nerve of an orientated block. The eyes are oriented in the blocks in order to always have VN and DT in opposite positions with respect to the optic nerve on sections. For quantification on retinal sections, 3 consecutive images for sample (as shown by the boxes 1, 2, 3) were taken in the VN side, then quantified and averaged. (B') Representative 60x confocal microscopy image from retinal section used for quantification. Ventro-nasal (VN), dorso-temporal (TD). *n*= 3 to 6 retinas were used for genotype. Scale bars: (A) 1 mm, (B) 0,5mm.

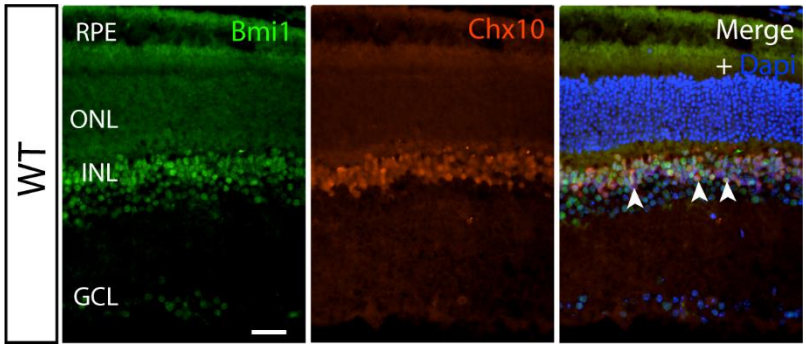

Figure S5. Bmi1 is highly expressed in bipolar neurons

IF analysis of a WT mouse retina (cryosections) using Chx10 and Bmi1 antibodies. Note Bmi1 expression in Chx10-positive cells of the INL. Retinal pigment epithelium (RPE); outer nuclear layer (ONL); inner nuclear layer (INL); ganglion cell layer (GCL). Scale bar: 20µm.

Figure S6. *Chk2* deletion partially improves the *Bmi1*$^{-/-}$ phenotype

Bmi1$^{-/-}$ */Chk2*$^{-/-}$ and *Chk2*$^{+/-}$ mice at P30. Note: *Bmi1*$^{-/-}$ */Chk2*$^{-/-}$ mice were healthier than *Bmi1*$^{-/-}$ mice but remained smaller than *Chk2*$^{+/-}$ control mice.

Table S1. Statistical analysis of ERG parameters

Global values from ERG experiment. Each parameter is analyzed by repeated measures ANOVA. The comparisons between the ERG parameters values at the Vmax are analyzed by one-way ANOVA. All values are mean ± SEM. N.S. = not significant; (*) P ≤ 0.05; (**) ≤ 0.01; (***) ≤ 0.001;

	Photopic system			Scotopic system		
	WT	+/-	-/-	WT	+/-	-/-
Overall a-wave amplitude	F(2,7) = 6.195, p = 0.028 *			F(2,7) = 1.297, p = 0.332 N.S.		
a-wave amplitude at Vmax	-215.4 ± 32.69 µV	-182.5 ± 15.29 µV	-88.35 ± 6.706 µV	-116.1 ± 12.17 µV	-117.4 ± 12.22 µV	-138.0 ± 10.05 µV
Comparison with the other groups (p-value)	+/- = 0.375 N.S.	WT = 0.375 N.S.	WT = 0.008 **	+/- = 0.939 N.S.	WT = 0.939 N.S.	WT = 0.226 N.S.
	-/- = 0.008 **	-/- = 0.039 *	+/- = 0.039 *	-/- = 0.226 N.S.	-/- = 0.281 N.S.	+/- = 0.281 N.S.
Overall a-wave implicit time	F(2,7) = 5.127, p = 0.043 *			F(2,7) = 0.596, p = 0.577 N.S.		
a-wave implicit time at Vmax	8.000 ± 0.4082 ms	8.667 ± 0.3333 ms	9.333 ± 0.3333 ms	21.75 ± 2.175 ms	19.67 ± 0.3333 ms	22.00 ± 2.517 ms
Comparison with the other groups (p-value)	+/- = 0.246 N.S.	WT = 0.246 N.S.	WT = 0.039 *	+/- = 0.484 N.S.	WT = 0.484 N.S.	WT = 0.932 N.S.
	-/- = 0.039 *	-/- = 0.275 N.S.	+/- = 0.275 N.S.	-/- = 0.932 N.S.	-/- = 0.464 N.S.	+/- = 0.464 N.S.
Overall b-wave amplitude	F(2,7) = 18.970, p = 0.001 ***			F(2,7) = 10.440, p = 0.008 **		
b-wave amplitude at Vmax	333.8 ± 34.78 µV	241.9 ± 17.32 µV	132.3 ± 9.479 µV	509.5 ± 24.04 µV	603.7 ± 51.01 µV	371.4 ± 40.33 µV
Comparison with the other groups (p-value)	+/- = 0.044 *	WT = 0.044 *	WT = 0.001 ***	+/- = 0.112 N.S.	WT = 0.112 N.S.	WT = 0.032 *
	-/- = 0.001 ***	-/- = 0.029 *	+/- = 0.029 *	-/- = 0.032 *	-/- = 0.004 **	+/- = 0.004 **
Overall b-wave implicit time	F(2,7) = 20.852, p = 0.001 ***			F(2,7) = 0.034, p = 0.966 N.S.		
b-wave implicit time at Vmax	27.25 ± 0.6292 ms	31.00 ± 1.000 ms	39.33 ± 2.848 ms	57.00 ± 1.472 ms	56.67 ± 1.453 ms	53.00 ± 2.517 ms
Comparison with the other groups (p-value)	+/- = 0.136 N.S.	WT = 0.136 N.S.	WT = 0.001 ***	+/- = 0.899 N.S.	WT = 0.899 N.S.	WT = 0.158 N.S.
	-/- = 0.001 ***	-/- = 0.010 **	+/- = 0.010 **	-/- = 0.158 N.S.	-/- = 0.217 N.S.	+/- = 0.217 N.S.